11th International Conference on Charged Particle Optics

from Oct. 15 to 18, 2024 in Fukui

CPO-11 ABSTRACT BOOKLET

Platinum Sponsors of CPO-11

The Japanese Society of Microscopy

ナノ荷電粒子ビーム産学連携委員会
The Japan Society of Applied Physics
Committee on Electron and Ion Beam Science for Nanotechnology

福井県公式観光サイト
ふくいドットコム
Fukui Prefectural Tourism Federation

Gold Sponsors of CPO-11

CEOS
Corrected Electron Optical Systems GmbH

MEBS
ELECTRON BEAM SOFTWARE

JEOL

Silver Sponsors of CPO-11

DAIWA
Daiwa Techno Systems

HITACHI
Inspire the Next

We would like to express our sincere gratitude to all the CPO-11 sponsors.

Local Organizing Committee
Yoichi Ose, Hitachi High Tech(Chair)
Ryuji Nishi, Fukui UT
Yasuhiko Sugiyama, Hitachi High Tech
Shin Fujita, Shimazu
Akira Yonezawa
Hidekazu Murata, Meijo U
Ryota Mishima, JEOL
Tadahiro Kawasaki, JFCC
Shigekazu Nagai, Mie U

Scientific Advisory Board
Martin Berz, Michigan State University, USA
Peter Hawkes, Toulouse, France
Georg Hoffstaetter, Cornell University, USA
Anjam Khursheed, Politecnico di Milano, Italy
Ondrej Krivanek, Nion, Kirkland, USA
Ali Gheideri, Delft University of Technology, Netherlands
Ilona Müllerová, ISI, Brno, Czech Republic
Eric Munro, MEBS, London, UK
Yoichi Ose, Hitachi High Tech., Ibaraki, Japan
Tomáš Radlička, ISI, Brno, Czech Republic
Harald Rose, University of Ulm, Germany
Gerd Schönhense, University of Mainz, Germany
Weishi Wan, ShanghaiTech University, China
Martin Winkler, GSI, Darmstadt, Germany
Hermann Wollnik, New Mexico State University, USA

We are pleased to announce that the 11th International Conference on Charged Particle Optics, CPO-11, hosted by Electron Optics Design Technology Subcommittee of JMS, will take place in Fukui-shi, Fukui, JAPAN, from Oct. 15 to 18, 2024. We welcome you to Fukui and look forward to meeting all of you at the conference.

History

The series of conferences on charged particle optics evolved from the realization that there is great overlap in techniques and tools among three until then somewhat separate communities using charged particle optics techniques: The fields of accelerator optics, spectrometer optics, and electron optics. Beginning in 1980, the first three meetings in the series were organized by Hermann Wollnik, Karl Brown, and Peter Hawkes, each a representative of one of these fields. Since then, the CPO conferences have continued their role as a bridge between these disciplines, and a total of ten conferences on Charged Particle Optics have been held:

1980 Giessen, Germany
1986 Albuquerque, NM, USA
1990 Toulouse, France
1994 Tsukuba, Japan
1998 Delft, Netherland
2002 College Park, MD, USA
2006 Cambridge, England
2010 Singapore
2014 Brno, Czech Republic
2018 Key West, FL, USA

Now four decades after the first meeting, the formula is as attractive as ever. In the spirit of continuing to bridge three related fields, we are now launching the 11th CPO conference, which will showcase a balanced program with much original material in each of the three areas.

CPO-11 Program

10/15(Tue)	Content	Presenter
PM1-2(13:30-17:30)	Venue preparation	
PM3(17:30-19:30)	Reception	Provided by JSM

10/16(Wed)		
9:00	Doors open	
AM1(9:15-10:20)	Session1(Time Resoled EM)	3 lectures chair(Ose, Berz)
9:15-9:20	Opening declaration	Yoichi Ose(Chair)
9:20-9:50	1 Invited lecture	Makoto Kuwahara(Nagoya Univ.)
9:50-10:20	2 Invited lecture	Yuya Morimoto(Riken)
(10:20-10:40)	Coffee Break 1	Provided by Hitachi High-Tech
10:40-11:10	3 Invited lecture	Ilona Müllerová(ISI CAS)
AM2(11:10-12:00)	Session2(Simulation1)	2 lectures chair(Ito, Fujita)
11:10-11:40	4 Invited lecture	John Rouse(MEBS)
11:40-12:00	5 General lecture	Hangfeng Hu(Xi'an Jiaotong Univ.)
(12:00-13:00)	Free Lunch 1	Provided by Fukui Prefectural Tourism Federation
PM1(13:00-15:10)	Session3(High Energy)	5 lectures chair(Rouse, Morimoto)
13:00-13:30	6 Invited lecture	Martin Berz(MSU)
13:30-14:00	7 Invited lecture	Kyoko Makino(MSU)
14:00-14:20	8 General lecture	Eremey V. Valetov(MSU)
14:20-14:40	9 General lecture	Eremey V. Valetov(MSU)
14:40-15:10	10 Invited lecture	Leon Bruckner(FAU)
(15:10-15:30)	Coffee Break 2	Provided by CEOS
PM2(15:30-17:00)	Session4(QEM & bord lecture on-line)	3 lectures chair(Blackburn, Enyama)
15:30-16:00	11 Invited lecture(Online)	Hiroshi Okamoto(Akita Prefectural Univ.)
16:00-16:30	12 Invited lecture	Sameen Ahmed Khan(Dhofar Univ.)
16:30-17:00	13 Invited lecture(Online)	Anjam Khursheed(Politecnico di Milano)
(17:00-18:00)		Move to Kaika-tei by yourself
PM3(18:00-20:00)	Banquet（Kaika-tei）	Supported by Fukui Prefectural Tourism Federation

10/17(Thu)		
9:00	Doors open	
AM1(9:15-10:05)	Session5(Electron source)	2 lectures chair(Nagai, Yamasaki)
9:15-9:45	14 Invited lecture	Lixin Zhang(IEE CAS)
9:45-10:05	15 General lecture	Jun Yamasaki(Osaka Univ.)
AM2(10:05-12:00)	Session6(Poster)	10 posters chair(Nishi)
10:05-10:55	Short presentation	5min＊10posters
(10:55-12:00)	Coffee Break 3	Provided by MEBS
10:55-12:00	Poster	10 poster presenters

CPO-11 Program

(12:00-13:20)	Lunch	Eating out on your own
13:20		Gather at the bus stop no.3
(13:30-18:00)	Excursion(Course A/B)	Supported by Fukui Prefectural Tourism Federation
(18:00-18:30)		Move to a bar by taxi or on hood
PM1(18:30-20:30)	Committee Meeting	Board and committee members

10/18(Fri)		
9:00	Doors open	
AM1(9:15-12:00)	Session7(Aberration Correction)	5 lectures chair(Makino, Mishima)
9:15-9:45	16 Invited lecture	Matthew R.C. Fitzpatrick(Uvic)
9:45-10:15	17 Invited lecture	Niklas Dellby(Bruker AXS)
(10:15-10:30)	Coffee Break 4	Provided by JEOL
10:30-11:00	18 Invitedlecture	Hiroyuki Ito(Osaka Univ.)
11:00-11:20	19 General lecture	Tomonori Nakano(Hitachi)
11:20-11:40	20 General lecture	Shun Kizawa(Hitachi)
AM2(11:35-12:05)	Session8(Mass)	1 lecture chair(Fujita, Khan)
11:35-12:05	21 Invited lecture	Dmitry Grinfeld(TFS)
(12:05-13:00)	Free Lunch 2	Provided by Fukui Prefectural Tourism Federation
PM1(13:00-15:00)	Session9(Simulation2)	5 lectures chair(Müllerová, Murata)
13:00-13:30	22 Invited lecture	Tomas Radlicka(ISI CAS)
13:30-14:00	23 Invited lecture	Martin Oral(ISI CAS)
14:00-14:20	24 General lecture	Rathaiah Pureti(LIST)
14:20-14:40	25 General lecture	Morimoto Takeshi(Hitachi)
14:40-15:00	26 General lecture	Yoichi Ose(HHT)
(15:00-15:10)	Closing	Yoichi Ose(Chair)
15:10-16:00	Withdrawal	

10/17(Thu)		
10:05-10:55	Short presentation	5min＊10posters
10:05	p01	Daichi Takane(Hitachi)
10:10	p02	Leon Bruckner(FAU)
10:15	p03	Shuhei Hatanaka(Osaka Univ.)
10:20	p04	Jiayu Li(Mie Univ.)
10:25	p05	Jintao Hu(XJTU)
10:30	p06	Yu Sato (Advantest)
10:35	p07	Shan Mei Li(XJTU)
10:40	p08	Yuto Suzuki(Meijo Univ.)
10:45	p09	Kazuhisa Sato(Osaka Univ.)
10:50	p10	Shinya Mizuno(Osaka Univ.)

Time-resolved transmission electron microscopy using a flat semiconductor photocathode with an NEA surface

Kuwahara, M. [1, a]
[1] Institute of Materials and Systems for Sustainability Nagoya University, Japan
[a] kuwahara@imass.nagoya-u.ac.jp

Dynamic observations of nanoscale materials provide important information for the time evolutions of optical couplings, phase transitions, and energy relaxations in a local site. Ultrafast measurement in electron microscopy using pulsed electron beams is a promising candidate for investigating high-speed phenomena on the nanoscale. Furthermore, high-brightness pulsed electron beam in transmission electron microscope (TEM) enables single-shot imaging, which is expected to observe biological specimens or organic material without electron-beam damage due to extracting information before thermalization of injected energy into specimen.

We had begun developing a spin-polarized pulse-TEM (SPTEM), which comprises a semiconductor photocathode with a negative electron affinity (NEA) surface for a polarized electron source and a 30-keV TEM [1]. The SPTEM showed that high-quality electron beam, e.g., high brightness, high spin-polarization, long coherent lengths, picosecond response time and narrow energy width, is realized by the semiconductor photocathode with an NEA surface (NEA-PC) in electron microscope [1,2]. However, observable thickness of specimen in the SPTEM is restricted due to the beam energy. Therefore, we have newly developed time-resolved TEM (TRTEM) using an NEA-PC as pulsed electron source equipped to the TEM column based on a 100-kV TEM instrument (HT7830, Hitachi High-Tech Corp.). The TRTEM is operated with beam energies of up to 100 keV, which improves transmittance in a specimen and provides higher brightness compared with previously developed 30-keV SPTEM. A thin GaAs film on a glass plate (Hamamatsu Photonics Inc.) was employed as a backside-illumination-type NEA-PC, and surface treatments of this photocathode were conducted in an NEA surface preparation system in the TRTEM. The electron beam was extracted from the flat surface of the photocathode with a high electric field gradient of 8 MV/m at an acceleration voltage of 100 kV along with suppression of the space charge effect (as a consequence of the high acceleration field gradient) [3].

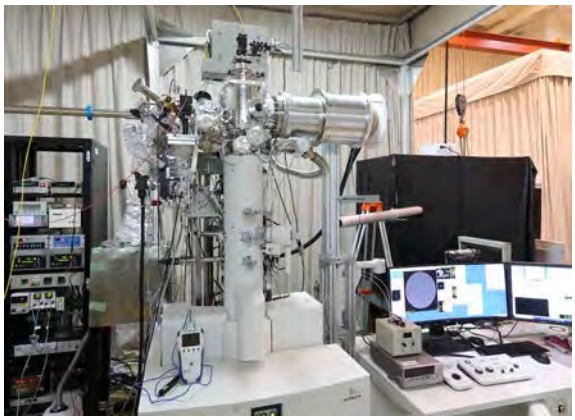

Figure 1. The newly developed 100 kV TRTEM system based on an HT7830 (Hitachi High-Tech Corp.).

Ultrafast phenomena in gold nanotriangles (AuNTs) stimulated by pulsed laser were investigated using transient electron energy-loss spectroscopy (TEELS) technique. Intensity enhancement and energy width broadening of the energy loss peak were observed at the EEL peaks associated with surface and bulk plasmons in the AuNTs [3]. The TEELS data showed two decay processes on decay-times of 7.8 ps and longer than 100 ps that compensated for the relaxation times of excited surface plasmons using transient absorption spectroscopy.

References:

[1] M. Kuwahara et al., Appl. Phys. Lett. **101**, (2012), 03310.
[2] M. Kuwahara et al., Appl. Phys. Lett. **105**, (2014), 193101.
[3] M. Kuwahara et al., Appl. Phys. Lett. **121**, (2022), 143503.

Optical-field-induced rocking-curve effect in attosecond electron diffraction

Morimoto, Y. [1,2,a] and Baum, P. [3]
[1] RIKEN Cluster for Pioneering Research (CPR) and RIKEN Center for Advanced Photonics (RAP), RIKEN, 351-0198, Wako, Saitama, Japan
[2] Department of Nuclear Engineering and Management, Graduate School of Engineering, The University of Tokyo, 7-3-1 Hongo, Bunkyo-ku, Tokyo 113-8656, Japan
[3] Universität Konstanz, Fachbereich Physik, 78464 Konstanz, Germany
[a] yuya.morimoto@riken.jp

Time-resolved electron microscopy has recently been advanced to the attosecond (1 attosecond = 10^{-18} second) resolution based on the novel technologies of laser-based temporal modulation [1,2], interferometry with optically-induced coherence [3,4] or sub-optical-cycle gating [5]. However, the spatial resolution is not at the atomic resolution yet. An approach for achieving both the atomic and attosecond resolution is the time-resolved diffraction using attosecond electron pulses [1,6].

In this presentation, we review our achievements on the production and direct characterization of attosecond electron pulses [1,7] and report our recent results of the attosecond transmission electron diffraction from a silicon crystal [6]. As shown in Fig. 1(a), a silicon membrane was excited by the electric field of laser light (red, 1030 nm, 0.2 V/nm amplitude) and the dynamics was investigated with the time-delayed attosecond electron pulse trains (blue). We observed periodic oscillations of the Bragg-spot intensities on the attosecond time scale, as shown in Fig. 1(b). We attributed the effect to the field-induced rocking-curve effect. The excitation field induces the quiver motion of the attosecond electron pulses and accordingly the incidence angle to the crystal is modulated on the ultrashort timescale, causing the decrease or increase of the Bragg-spot intensities due to the rocking-curve effect. We discuss how to disentangle the signals originating from the electronic motion in a sample from the rocking-curve effect [6]. The field-induced rocking curve effect needs to be considered in future attosecond electron microscopy and diffraction experiments.

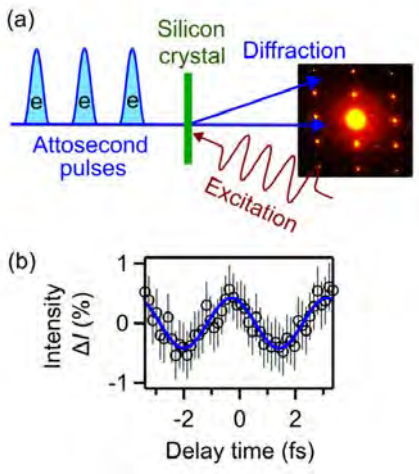

Figure 1. Attosecond electron diffraction experiment [6].

References:

[1] Y. Morimoto and P. Baum, *Nat. Phys.* **14**, 252–256 (2018).
[2] D. Nabben et al., *Nature* **619**, 63–67 (2023).
[3] J. H. Gaida et al., *Nat. Photon.* **18**, 509–515 (2024).
[4] T. Bucher et al., *Nat. Photon.* **18**, 809–815 (2024).
[5] D. Hui et al., *Sci. Adv.* **10**, 5805 (2024).
[6] Y. Morimoto and P. Baum, *Phys. Rev. Lett.* **132**, 216902 (2024).
[7] Y. Morimoto and P. Baum, *Phys. Rev. Lett.* **125**, 193202 (2020).

Time-of-Flight spectrometer for low landing energies in SEM

Müllerová, I.[1, a], Konvalina, I.[1], Paták, A.[1], Průcha, L.[1], Piňos, J.[1], Zouhar, M.[1], Materna Mikmeková, E.[1]
[1] Institute of Scientific Instruments of the Czech Academy of Sciences, Czech Republic
[a] ilona.mullerova@isibrno.cz

Two-dimensional (2D) materials have recently gained significant popularity due to their interesting properties and extensive application potential. Advances in the production of high-quality 2D materials have highlighted the need for detailed study and analysis.

To enhance our understanding of contrast formation in the energy range below 100 eV, it is essential to deepen our knowledge of how (very) low energy electrons interact with solids. Accurate description of electron transport in and across the sample interface region is vital for obtaining precise quantitative information. In this context, the inelastic mean free path, which characterizes electron scattering, is a critical parameter. This information will be provided by a newly developed ultra-high vacuum scanning low energy electron microscope. The device features a time-of-flight (ToF) spectrometer that operates in transmission mode, enabling the use of both scanning electron microscopy and spectroscopy at the same time [1].

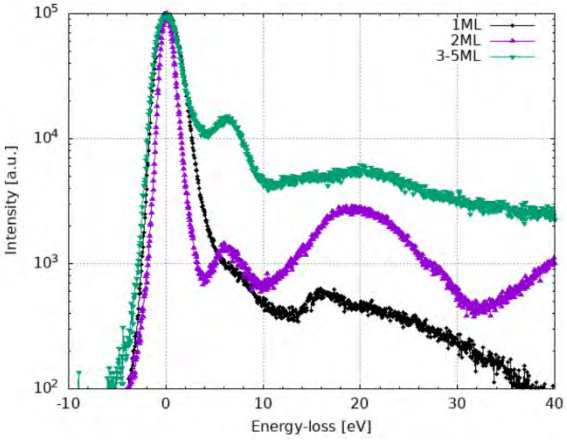

Figure 1. EELS spectra for a graphene sample with a constant landing energy of 100 eV, varying the number of layers.

Graphene, a prominent 2D material, is celebrated for its lightweight nature, exceptional tensile strength, and distinctive properties such as outstanding electrical and thermal conductivity and transparency. These attributes make it an ideal candidate for investigation at very low energies using the transmission mode of our device. We performed experiments with commercial graphene samples (Ted Pella, Inc.) to acquire electron energy loss spectra (EELS), Figure 1.

In this study, we analyse experimental spectra of graphene and other 2D materials obtained at low landing energies. The measured data are compared with simulated momentum-resolved EELS using many-body perturbation theory, Yambo code, on top of density-functional theory, Quantum Espresso [2]. These theoretical investigations offer valuable insights into the experimental results.

References:
[1] Konvalina, I. et al., Nanomaterials 11 (9), 2435 (2021).
[2] Giannozzi, P. et al., J. Phys. Condens. Matter 21, 395502 (2009).

Acknowledgement: This research was supported by the Czech Science Foundation, grant number GA22-34286S, together with institutional support RVO:68081731.
The authors thank Prof. Kenji Matsuda from the University of Toyama for his long-standing collaboration.

Computing Initial Energy Distributions for Field Emission Sources

John Rouse [a] and Catherine Rouse

Munro's Electron Beam Software Ltd., London, UK.

[a] john@mebs.co.uk

In the simulation of electron sources, it is often necessary to perform a Monte Carlo analysis of the beam properties. To do this, the random initial conditions of the particles at the cathode surface, including the positions and velocity components, need to be generated.

The velocity components obey the initial energy distribution of the source. For various emission mechanisms, the initial energy probability distributions, $g(E)$, are theoretically well established [1] [2].

To generate the energy distribution numerically, the probability density must be integrated so that the distribution can be inverted. Once this is done, a random uniform deviate can be generated to give a random initial energy of the desired distribution.

For thermionic emission, the integral of the probability distribution can be done analytically using simple trigonometric functions. In many sources, however, the emission mechanism is field emission or thermal field emission types. In these cases, it is not so straightforward to integrate the probability distribution analytically.

In this paper, we will show how we have derived analytic formulae for the integrals of the energy probability distributions for cold and thermal field emission sources. For cold field emission, we prove that the integral of the probability distribution can be written in the form:

$$\int g(E)\,dE = \frac{\sin(\pi p)}{\pi p} e^{E/d}\,{}_2F_1(1, p; p+1; -e^{E/pd})$$

where ${}_2F_1$ is the Gaussian hypergeometric function. Similarly, for extended Schottky emission, we prove that the integral of the probability distribution can be written in the form:

$$\int g(E)\,dE = \frac{\sin(\pi q)}{\pi q} e^{\frac{-(E-W_F)}{kT}} \left[{}_2F_1\left(1, -q; 1-q; -e^{\frac{-(E-W_F)}{qkT}}\right) - q \ln\left[1 + e^{\frac{-(E-W_F)}{qkT}}\right] - 1 \right]$$

The Gaussian hypergeometric function, ${}_2F_1$, can be evaluated numerically using established techniques [3], just like calling a trig function, for example. Hence, the random energy, and therefore velocity components, can be generated efficiently for the many thousands of particles typically needed for a Monte Carlo analysis of the source.

We have implemented these integrals in a computer program and will demonstrate the generation of sets of particles whose initial energy fit the desired distribution for field emission sources.

References:

[1] P.W. Hawkes & E. Kasper, "Principles of Electron Optics", Vol. 2, Chapter 44 (2018)
[2] L. Swanson and A. Bell, "Advances in Electronics and Electron Physics", Vol. 32 (1973)
[3] W.H. Press, et al, Numerical Recipes in C++ Third Edition, CUP (2007)

Aberration Analysis and Design Method of Array Deflector for Variable-Axis Lens System Based on the Differential Algebra Method

Hu, H.F. [1, a], Kang, Y.F. [1]
[1] Key Laboratory for Physical Electronics and Devices of the Ministry of Education, School of Electronic Science and Engineering, Xi'an Jiaotong University, People's Republic of China
[a] huhangf362@stu.xjtu.edu.cn

The variable-axis lens (VAL) can essentially eliminate off-axis aberrations by shifting the electron-optical axis in synchronism with the deflected beam [1]. However, in VAL system (Figure 1), the rotationally symmetric field of compound electrostatic-magnetic lens is coupled with the dipole field of deflector, which causes both curvature and torsion of electron beam optical axis [2]. The traditional electron optical calculation theory is forced to adopt paraxial approximation to obtain the variable axis condition, and the off-axis aberration is analyzed by the series expansion of electromagnetic field based on the straight optical axis. As the off-axis distance increases, the series becomes difficult to converge.

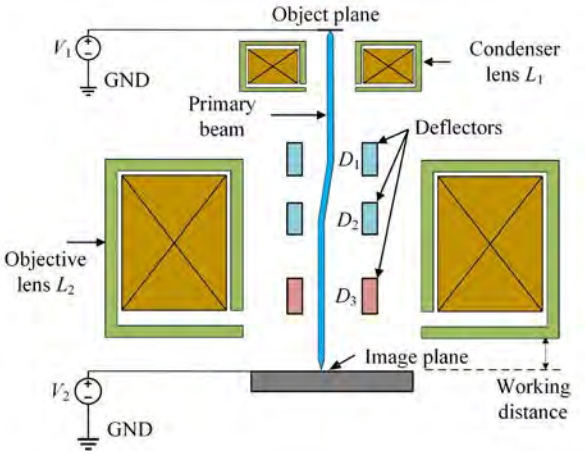

Figure 1. The scheme of the VAL system.

In this study, a high-order aberration calculation method for VAL system based on the differential algebra method is established firstly. A high-precision local analytical expression for the harmonic components of the electromagnetic field in the VAL system is constructed and it is converted into DA quantity. An off-axis reference trajectory is traced and the high-order aberrations referring to the off-axis trajectory are obtained. It solves the problems of traditional method being difficult to handle the off-axis high-order aberration calculation [3]. Then, the influence of working distance and landing energy on electron optical properties in retarding field VAL system is studied. As the working distance increases and the landing energy ascends, the off-axis dispersion and second-order aperture aberration will decrease and gradually tend to stable. Finally, a design method for array type electrostatic deflector in VAL system is proposed. By using the least squares method to optimize excitation of each deflector cell, the off-axis focusing error, dispersion and second order aperture aberration coefficients are improved.

References:
[1] Pfeiffer H.C. et al., Appl. Phys. Lett., 39, 775-776 (1981).
[2] Piles E., Ultramicroscopy, 93, 305-319 (2002).
[3] Zhao J.Y. et al., Nucl. Instrum. Methods Phys. Res. Sect. A, 1048, 167921 (2023).

Acknowledgments:
This work was supported by the National Natural Science Foundation of China (Grant No. 62071372) and the Natural Science Basic Research Program of Shaanxi (Program No. 2024JC-JCQN-69).

Nonlinear Effects in Single Pass versus Multi Pass Systems, What is Common and What is Different.

Berz, M[1, a]
[1] Michigan State University, USA
[a] berz@msu.edu

Compared to single pass systems like those used in microscopy and spectroscopy where careful consideration and control of aberrations is important, in multi pass system other priorities arise. This is largely due to the fact that many of the aberrations cancel out when traversing a system repeatedly, which is greatly helped by the adjustment of the linear transfer matrix to be non-resonant. However, some other effects have a tendency to build up over time either linearly or exponentially, and a specific form of analysis is necessary to understand and control this behavior. This is achieved using normal form methods which allow a clear separation of multi pass effects that are transient and those that are persistent, as well as the use of symplectic integration.

The DA methods employed in COSY INFINITY allow for the computation of aberrations of arbitrary order and also the relevant normal forms. The tools also allow the automatic computation of fully Maxwellian 3D fields if only midplane or on-axis field information is available, which for example allows recovering all nonlinear effects arising from increasing or decreasing fields in the fringes of particle optical elements. They also allow the computation of such fields from surface or volume field measurements, leading to a fully Maxwellian representation even in the presence of noise in the data. Utilizing metrics on symplectic spaces, it is possible to construct minimally invasive symplectification schemes for study of multi pass systems based on maps. Various examples of the performance of the methods are given, with particular emphasis on the high accuracy requirements of the spin and orbit dynamics of the FNAL muon g-2 ring.

Rigorous Computations of High-Order Aberrations

Makino, K. [1, a], Berz, M. [1]
[1] Michigan State University, USA
[a] makino@msu.edu

High-order transfer maps offer many advantages in the study of both single-pass systems, where they represent optical aberrations, and multi-pass systems, where they allow the direct computation of relevant properties like high-order dispersions, chromaticities, and amplitude- and parameter dependent tune shifts. They also allow for symplectic tracking even for very complicated systems that cannot be described by inherently symplectic kicks and related methods. However, one remaining question is always how accurate a map of a given expansion order really is – while in many cases, the sizes of high order contributions decrease as a function of order, this does not always have to be the case, for example for the muon g-2 ring, strong nonlinearities newly arise at order 9 and beyond.

In this talk, we present methods to determine mathematically rigorous bounds on all missing orders beyond the one explicitly considered. The computational effort to determine these bounds is small compared to the cost of the underlying high-order transfer map computation.

Advances in Beam Dynamics Simulations for the Muon g-2 Experiment

Valetov, E.V.[1,a]
[1] Michigan State University, USA
[a] evv@msu.edu

The Muon g-2 Experiment (E989) at Fermilab aims to measure the muon anomalous magnetic moment a_μ with unprecedented precision of 140 ppb using a storage ring, potentially leading to experimental indications of Beyond-the-Standard-Model particle physics. The result of Runs 1-3 was published in 2023 with a precision of 200 ppb. The experiment pushes the limits in terms of accuracy and systematic errors. Beam dynamics corrections are necessary to accommodate muons not orbiting exactly in the midplane, their oscillations, electric field effects, and various aberrations. Highly accurate beam dynamics models and simulations are crucial for quantifying and validating these corrections, facilitating the achievement of the 70-ppb systematic uncertainty that is necessary for the 140-ppb final total precision. A hybrid high-statistics simulation approach is being developed that uses the Geant4-based raytracing code gm2ringsim for about the first 30 turns in the storage ring after injection, where modelling the interaction of some of the injected beam with the CAD-based geometry is a priority, while leveraging the highly accurate and efficient tracking using the code COSY INFINITY between about 30 and 2000 turns after injection. The code COSY INFINITY uses precise fringe field calculations, advanced symplectification methods, and high-order differential-algebraic transfer maps to handle high-order aberrations. The COSY INFINITY model incorporates the measured magnetic field data and a multipole expansion of the Muon g-2 high voltage electrostatic quadrupole up to the duodecapole. The experiment completed its final Run 6 in July 2023, collecting 21 times more data than the previous Muon g-2 experiment at Brookhaven National Laboratory. Analyses of data from Runs 4-6 are ongoing, with results planned for release in 2025.

Beam Dynamics Design of a Second Order Achromat for Electron Radiography

Valetov, E.V.[1,2,a]
[1] Michigan State University, USA
[2] Los Alamos National Laboratory, USA
[a] evv@msu.edu

We performed the beam dynamics design of a 5-cell second-order 25 MeV electron achromat as a prototype for an 800 MeV proton achromat for a next-generation proton radiography (pRad) facility. The achromat has a modular design comprising cost-effective, low-complexity elements. The achromat layout was scaled and optimised with the constraint of fitting an experimental area at the Idaho Accelerator Center (IAC). While the achromat is second order in principle, aberrations up to the fifth order were considered in optimisation to ensure high fidelity imaging. We used the code *COSY INFINITY* for accurate beam dynamics simulations and fitting, in combination with optimisation of some parameters using asynchronous Bayesian optimisation provided by the tool *DeepHyper*. We carried out acceptance, sensitivity, chromaticity, fringe field effects, Fourier plane location, and other studies to characterize the achromat's performance and identify potential limitations. We simulated the imaging of a step wedge using the codes *G4beamline* and *MARS* to validate the design's imaging capabilities. The achromat was assembled at the IAC and is being prepared for operation. This prototype represents a significant step towards the development of advanced imaging capabilities for a next-generation pRad facility, aiming to enable higher resolution and more detailed studies of dynamic events in dense materials.

Accelerating and guiding electrons with optical forces

Brückner, L. [1,a], Chlouba, T. [1], Shiloh, R. [1,2], Kraus, S. [1], Litzel, J. [1], Zhao, Z. [1], Konrad, M. [1], Morimoto, Y. [1,3], Hommelhoff, P. [1]
[1] Physics Dept., Friedrich-Alexander-Universität Erlangen-Nürnberg, Erlangen, Germany
[2] Dept. of Applied Physics, Hebrew University, Jerusalem, Israel
[3] RIKEN, Wako, Saitama, Japan
[a] leon.brueckner@fau.de

Dielectric laser acceleration (DLA) is a scheme to accelerate electrons with light fields at dielectric nanostructures. The high peak fields provided by femtosecond infrared laser systems combined with the high damage threshold of dielectric materials allows for high acceleration gradients and thus a path towards the miniaturization of particle accelerators. [1]

The nanometric dimensions of the accelerator (225 nm channel width) necessitate dynamic beam control over short length scales. To this end, we utilize the optical forces exerted by the incoming laser field. By incorporating gaps into the structure, electrons can jump between two phases of the synchronous light field, leading to an alternation between focusing and defocusing forces and a net guiding effect [2]. We note that the focusing strength in the DLA structure can reach MT/m, far exceeding that of conventional magnetic quadrupoles [3].

Combining this guiding scheme with a tapering of the structure period enables us to coherently guide and simultaneously accelerate an electron bunch over long distances [4,5] (Figure 1). We have achieved an energy gain of 12.3 keV, or 43% of the input energy, in a 500 µm long silicon DLA, corresponding to an acceleration gradient of 23 MeV/m (Figure 2).
Significant increases in the acceleration gradient are possible through the use of mid-infrared excitation wavelengths [6]. These results open the door towards future high-gradient, miniaturized, on-chip particle accelerators.

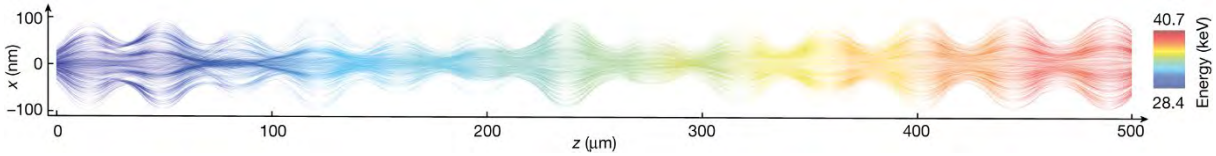

Figure 1: Simulated beam trajectory in the 500 µm accelerator structure [4].

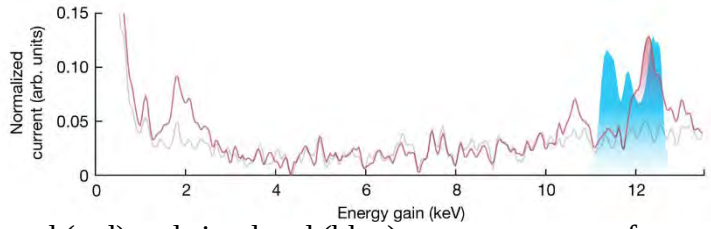

Figure 2: Measured (red) and simulated (blue) energy spectrum from a 500 µm long DLA [4].

References:

[1] R. Shiloh, N. Schönenberger, Y. Adiv, R. Ruimy, et al., Adv. Opt. Phot. 14, 862 (2022)
[2] R. Shiloh, J. Illmer, T. Chlouba, P. Yousefi, et al., Nature, 597, 498-502 (2021)
[3] D. S. Black, K.J. Leedle, Y. Miao, et al., Phys. Rev. Lett. 122, 104801 (2019)
[4] T. Chlouba, R. Shiloh, S. Kraus, L. Brückner, J. Litzel, et al., Nature, 622, 476 (2023)
[5] P. Broaddus, T. Egenolf, D.S. Black, M. Murillo, et al., Phys. Rev. Lett. 132, 085001 (2024)
[6] L. Brückner, T. Chlouba, Y. Morimoto, et al., Optics Express, 32, 16, 28348-28355 (2024)

Quantum Charged-Particle Optics: Current Status and Future Perspective

Okamoto, H.[1, a]
[1] Department of Intelligent Mechatronics, Akita Prefectural University, Japan
[a] okamoto@akita-pu.ac.jp

A variety of quantum-enhanced measurement technologies are being developed in recent years. Charged particle optics occupies a special place in the spectrum, since it comes with a unique set of applications and enabling experimental techniques. In particular, low-dose imaging of biological specimens would be an important application of quantum-enhanced measurement [1]. This field used to be heavily theoretical, but interesting experimental results now begin to appear [2, 3].

In this talk, I first review what has been going on in the field of quantum charged particle optics. This is followed by a discussion of a particular line of theoretical research that our group has been pursuing: Namely, the use of superconducting quantum devices as a new tool in charged particle optics [4-5]. To elaborate, superconducting quantum devices, such as superconducting qubits, has the remarkable property to generate a *quantum mechanically superposed electromagnetic field* around them. A charged particle interacts with such a field in ways that have not happened in charged particle optics thus far. This would, as a non-trivial consequence, lead to a measurement scheme going beyond the shot noise limit, which should benefit low-dose imaging (Figure 1). Finally, I would take the liberty of speculating about the future directions that this field might take.

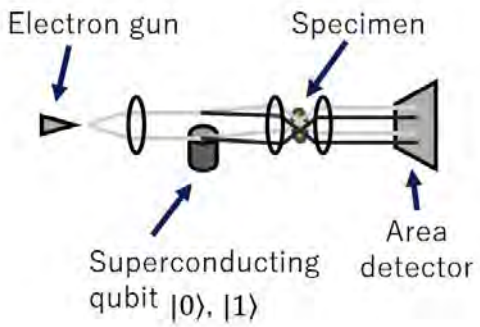

Figure 1. A 4D-STEM with its scanning coil replaced by a super-conducting qubit.

References:

[1] Kruit, P. et al., Ultramicroscopy **164**, 31 (2016).
[2] Koppel, S.A. et al., Ultramicroscopy **207**, 112834 (2019).
[3] Turner, A.E. et al., Phys. Rev. Lett. **127**, 110401 (2021).
[4] Okamoto, H. Phys. Rev. A **85**, 043810 (2012).
[5] Okamoto, H. arXiv:2209.04819[quant-ph] (2022).

Acknowledgment
I thank all the students, collaborators and colleagues involved in our work over the years. They include Takumi Higuchi, Yuki Okuda, Yukihiro Takayama, Shigeo Miura, Ismet Kaya, Marek Malac, and Yukinori Nagatani. This research was supported in part by the JSPS “Kakenhi” grant (#19K05285).

Quantum Charged Particle Beam Optics

Sameen Ahmed Khan[1, a], Ramaswamy Jagannathan[2]
[1] Dhofar University, Salalah, Sultanate of Oman
[2] The Institute of Mathematical Science, Chennai, India
[a] rohelakhan@yahoo.com

Though the classical charged-particle beam optics is very successful, in designing and operating numerous charged-particle beam devices from electron microscopes to particle accelerators, it is natural to look for the quantum theory of such systems handling beams of microscopic particles for which quantum mechanics should be relevant. With the curiosity of understanding how the classical charged particle beam optics is so successful, the quantum charged particle beam optics (QCPBO) is being developed by Jagannathan et al. QCPBO is seen to reproduce the classical charged-particle beam optics exactly for the paraxial and aberrating systems in the classical limit of dropping the additional quantum correction terms which depend on the Planck constant and are, of course, extremely small compared to the classical terms. In the classical limit, the quantum formalism reproduces the well-known Lie algebraic formalism of classical charged-particle beam optics. QCPBO based on the Klein-Gordon equation is applicable to spin-0 and spin-less particles. The formalism of QCPBO based on the Dirac equation provides a unified treatment of orbital and spin dynamics of a Dirac particle with anomalous magnetic moment being transported through magnetic optical elements accounting for the orbital phase-space transfer maps, including the Stern-Gerlach effect, and the Thomas-Bargmann-Michel-Telegdi spin motion.

References:

[1] R. Jagannathan, R. Simon, E.C.G Sudarshan, N. Mukunda, Quantum theory of magnetic electron lenses based on the Dirac equation, *Physics Letters*, **A134**, 457-464 (1989).
[2] R. Jagannathan, Quantum theory of electron lenses based on the Dirac equation, *Physical Review*, A42, 6674-6689 (1990).
[3] R. Jagannathan and S.A. Khan, Quantum theory of the optics of charged particles, *Advances in Imaging and Electron Physics*, **97**, 257-358 (1996).
[4] S.A. Khan and R. Jagannathan, On the quantum mechanics of charged particle beam transport through magnetic lenses, *Physical Review*, **E51**, 2510-2515 (1995).
[5] M. Conte, R. Jagannathan, S.A. Khan and M. Pusterla, Beam optics of the Dirac particle with anomalous magnetic moment, *Particle Accelerators*, 56, 99-126 (1996).
[6] S.A. Khan, Quantum theory of charged-particle beam optics, University of Madras, Chennai, India, 1997 (PhD thesis).
[7] S.A. Khan, The Foldy-Wouthuysen Transformation Technique in Optics, *Advances in Imaging and Electron Physics*, **152**, 49-78 (2008).
[8] R. Jagannathan and S.A. Khan, *Quantum Mechanics of Charged Particle Beam Optics, Understanding Devices from Electron Microscopes to Particle Accelerators*, CRC Press, Taylor & Francis (2019).
[9] S.A. Khan and R. Jagannathan, Quantum mechanics of bending of a nonrelativistic charged particle beam by a dipole magnet, *Optik*, **206**, 163626 (2020).
[10] S.A. Khan and R. Jagannathan, Classical and quantum mechanics of the Wien velocity filter, *International Journal of Theoretical Physics*, **63** (1), 16 (2024).
[11] S.A. Khan and R. Jagannathan, Quantum mechanics of bending of a charged particle beam by a dipole magnet, *Advances in Imaging and Electron Physics*, **229**, 1-41 (2024).

The challenges and opportunities for nanoscale mapping of band-structure using a scanning electron microscope

Anjam Khursheed[1,a], Silvia Maria Pietralunga[2], and Alberto Tagliaferri[1]
[1]Department of Physics, Politecnico di Milano, Milan, Italy.
[2]Consiglio Nazionale delle Ricerche (CNR), Italy.
[a] anjam.khursheed@polimi.it

The possibility of developing scanning electron microscopes (SEMs) to map band-structure on the nanoscale is not widely known. The recent capture of accurate bulk valence band density of states (DOS) information in a commercial scanning electron microscopy (SEM) using secondary electron energy spectroscopy (SEES) has created new directions of development for the characterization of nanomaterials [1]. Close agreement between experimental and theoretical valence band DOS distributions was obtained for six different test planar samples, consisting of 5 metals and one semiconductor, where the normalized root mean square deviation ranged from 2.7 to 6.7%. Figure 1 presents a schematic diagram of the SEES analyzer attachment setup that was used inside the SEM together with its results for a bulk gold test specimen. This is the first time that the shape of the valence band DOS distribution has been accurately captured by the SEES technique, and it is the first time that SEES has been successively demonstrated in the specimen chamber of a SEM.

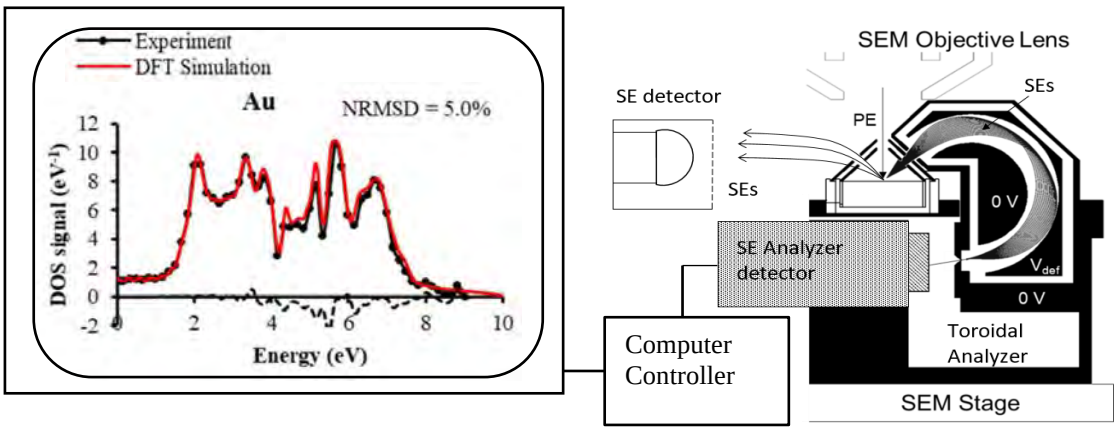

Figure 1. Schematic layout of a SEES analyzer attachment inside a SEM and its experimental valence band density of states (DOS) distribution compared to DFT simulations for a bulk test gold specimen.

This paper will review the potential of using the SEES technique in the SEM and examine the challenges and opportunities for using it to achieve nanoscale mapping of band-structure information. The possibility of creating a SEES-SEM momentum microscope will be discussed and compared to present state-of-the-art methods based upon photon beams, such as micro angle-resolved photon electron spectroscopy (ARPES), and Photoemission electron microscope (PEEM) ARPES.

References:

[1] W. Han et al., Scientific Reports, **10**, 22144 (2020).

Development of the multi-beam electron source based on thermal field electron gun

Lixin Zhang[1,a], Weixia Zhao[1], Junbiao Liu[1], Bohua Yin[1], Li Han[1]
[1] Institute of Electrical Engineering Chinese Academy of Sciences, Beijing 100190, China
[a] e-mail address : zhanglx@mail.iee.ac.cn

Since the advent of the first transmission electron microscope, microscopic imaging technology of the single-beam electron beam has been developed for more than 90 years. In recent years, high-throughput, large-area microscopic imaging based on multiple electron beams has been developed significantly[1][2], which has promoted the development of the related fields, such as life sciences, neuroscience, and semiconductors[3][4].

A multi-beam electron source based on a thermal field electron gun has been being developed in our group. An electrostatic collimating lens is added below the extractor to obtain the collimated electron beam. An aperture array and an arrayed electrostatic lens for multi-beam focusing are developed based on MEMS technology. In order to achieve high-precision (<500nm) assembly of the MEMS devices, we developed an assembly system for multi-aperture, multi-layer device and successfully achieved high-precision assembly with an error of less than 200 nm. The MEMS device is combined with the collimating lens to form the collimation, beam splitting and focusing of the 3×3 electron beams, and the spot size can be adjusted successfully (shown in Fig 1).

At this moment, the spot size and current distribution are being tested.

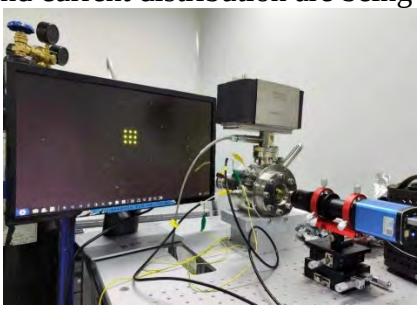

Fig 1 Experimental setup of multi-beam electron source

References:
[1] Eberle A. L., Schalek R., Lichtman J. W. et al. Multiple-Beam Scanning Electron Microscopy[J]. Microscopy today, 2015, 23(2): 12-18.
[2] Kruit P., Zuidema W. A Dedicated Multi-Beam SEM for Transmission Imaging of Thin Samples[J]. Microscopy and Microanalysis, 2019, 25(S2): 1034-1035.
[3] Eberle A. L., Zeidler D. Multi-Beam Scanning Electron Microscopy for High-Throughput Imaging in Connectomics Research[J]. Front Neuroanat, 2018, 12: 112.
[4] Sanchez M. I., Ukraintsev V. A., Neumann J. T. et al. High-throughput multi-beam SEM: quantitative analysis of imaging capabilities at IMEC-N10 logic node[C]. presented at the Metrology, Inspection, and Process Control for Microlithography XXXI, 2017.

Acknowledgments: This work was financially supported by the Research Instrument and Equipment Development Project of Chinese Academy of Sciences (Grant No: GJJSTD20200003) and the National Natural Science Foundation of China (Grant No: 62101528).

Measuring Spatial Coherence of Electron Beams in TEM by Analyzing Airy Diffraction Patterns

Jun Yamasaki[1, 2, a] and Shuhei Hatanaka[1]
[1] Research Center for Ultra-High Voltage Electron Microscopy, Osaka University, Japan
[2] Institute of Materials and Systems for Sustainability, Nagoya University, Japan
[a] yamasaki@uhvem.osaka-u.ac.jp

Partial spatial coherence of electron beams imposes limitations in various imaging/diffraction methods in transmission electron microscopes (TEMs), such as high-resolution TEM/STEM, off-axis electron holography, and electron diffractive imaging. Quantitative evaluations of the beam coherence are one of the important issues for the correct interpretation of the experimental data and enhanced quality by proper processing. We have developed a method to measure the spatial coherence in electron beams based on analysis of the Airy diffraction pattern from a selector aperture [1-3]. The method does not require an electron biprism and can be implemented in existing analytical TEMs equipped with a post-column energy filter.

Figure 1(a) shows a small-angle scattering pattern from a circular selector aperture (Airy diffraction pattern), which was precisely recorded at an extended camera length utilizing the additional magnification in a post-column energy filter. The elongation of the main peak is owing to 2-fold astigmatism of the lens system. As shown in Fig. 1(b), the experimental pattern is well reproduced by a fitting calculation considering various parameters such as geometric/chromatic aberrations of the lens system and the point-spread function (PSF) of the diffraction blurring. Analyzing the PSFs depending on the beam diameters, components that are attributed to the partial spatial coherence are successfully separated from the PSFs.

Figure 1(c) shows the spatial coherence length measured in 200-kV TEMs equipped with a Schottky field-emission gun (FEG), a cold FEG, and a LaB_6 thermionic gun. In each TEM, linear relationships between the spatial coherence length and the beam diameter at the specimen plane were observed as predicted theoretically [4]. The difference of the inclination of the linear lines was successfully converted to the difference in the brightness between each emitter in further analysis [4, 5].

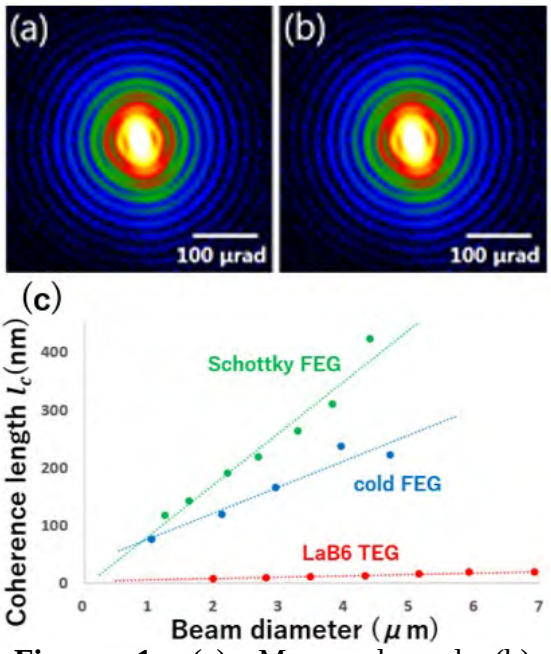

Figure 1. (a) Measured and (b) calculated Airy diffraction pattern. (c) Spatial coherence length depending on the beam diameter.

References:
[1] S. Morishita, J. Yamasaki, and N. Tanaka, Ultramicroscopy, **129** (2013) 10-17.
[2] J. Yamasaki et al., Microscopy **67** (2018) 1-10.
[3] S. Hatanaka and J. Yamasaki, J. Opt. Soc. Am. A**38** (2021) 1893-1900.
[4] S. Hatanaka and J. Yamasaki, Microscopy (2024), doi.org/10.1093/jmicro/dfae040.
[5] S. Hatanaka and J. Yamasaki, Phys. Rev. A **110** (2024) 013702.

Measurement and Correction of Lens Distortions Using Deep Learning on Convergent Beam Electron Diffraction Data

Fitzpatrick, M.R.C.[1, a], Blackburn, A.M. [1]
[1] Centre for Advanced Materials and Related Technologies and Department of Physics and Astronomy, University of Victoria, BC, Canada.
[a] mrfitzpa@uvic.ca

Recently developed 4-dimensional scanning transmission electron microscopy (4D-STEM) techniques collect large electron diffraction datasets to determine, for example, micro-structural and orientation information, and high-resolution phase-amplitude imagery through ptychography. However, the accuracy of these techniques is limited by the lens-induced optical distortion in the diffraction data. Optical distortions are hard or sometimes impossible to physically eliminate for few projector lens STEM instruments, particularly at low beam energies where scattering angles are increased.

Existing electron diffraction distortion characterization techniques typically use a known material system, to allow comparison between experimental and model data [1]. However, accurate localization of experimental convergent beam electron diffraction (CBED) disks is complicated by overlapping CBED disks, and distortion fields producing non-elliptical disks. To overcome these limitations and develop a method that does not require a known fixed sample, we produce a deep learning (DL) model to take as input a CBED pattern, and return as output the distortion field. To train our model we use basic mathematical objects to imitate CBED patterns. After obtaining the estimated distortion field, we perform backward mapping to generate distortion-corrected diffraction data.

We tested our DL model using distorted CBED patterns produced from multi-slice simulations of multiple-layer MoS_2. For the majority of the test images, our model predicts correctly the distortion field with a root-mean-squared error (RMSE) less than 2% (Figure 1).

Our DL model offers a quick and facile way of extracting higher-order distortion coefficients, including those of barrel-pincushion, spiral, elliptical, and parabolic distortion, from experimental CBED patterns, without requirements for any particular reference sample. A pre-trained model along with the related Python-based code used to measure and correct for distortion will be made available for public use on GitHub [2], and we anticipate that it will have wide applications in improving the accuracy of electron diffraction based techniques.

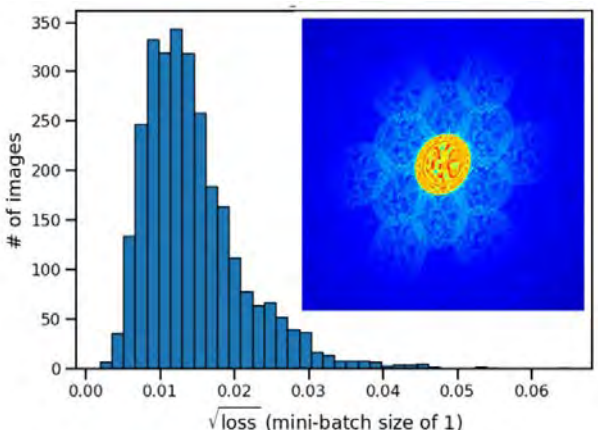

Figure 1. Histogram of the RMSE of the DL model extracted distortion field as a percentage of the image width. Inset: A sample 512x512 pixel test CBED pattern.

References:

[1] Mahr, C., et al., Ultramicroscopy 196, p. 74-82 (2019).
[2] Fitzpatrick, M.R.C., https://github.com/mrfitzpa/emnn (2024).

Double Sided Secondary Electron Imaging With Atomic Resolution in a STEM

B. Plotkin-Swing[1]*, J. Martis[1]*, C. Su[2], M.T. Hotz[1], N. Dellby[1], T. Radlička [3], O.L. Krivanek[1], T. C. Lovejoy[1]
[1] Bruker AXS (formerly Nion R&D), Kirkland, WA, USA
[2] Dept. of Mechanical Engineering and Materials Science, Yale University, New Haven, CT
[3] Institute of Scientific Instruments of Czech Academy of Sciences, Brno, Czech Republic
Niklas.Dellby@Bruker.com

Secondary electron (SE) imaging offers surface sensitivity which is complementary to the projected view provided by most scanning transmission electron microscope (STEM) techniques. We have added SE detectors below and above the specimen to a Nion HERMES STEM, opening the possibility of imaging the entrance[1] and exit surfaces of transmissive samples simultaneously with other STEM data channels.

The Nion STEM has a UHV (~10-9 torr) and an in-situ laser-based sample cleaning capability. The laser directly illuminates a ~20 µm diameter area of the sample around the probe location, allowing the area of interest to be heated while it is being imaged; this capability has proved invaluable for cleaning monolayers and bilayers[2].

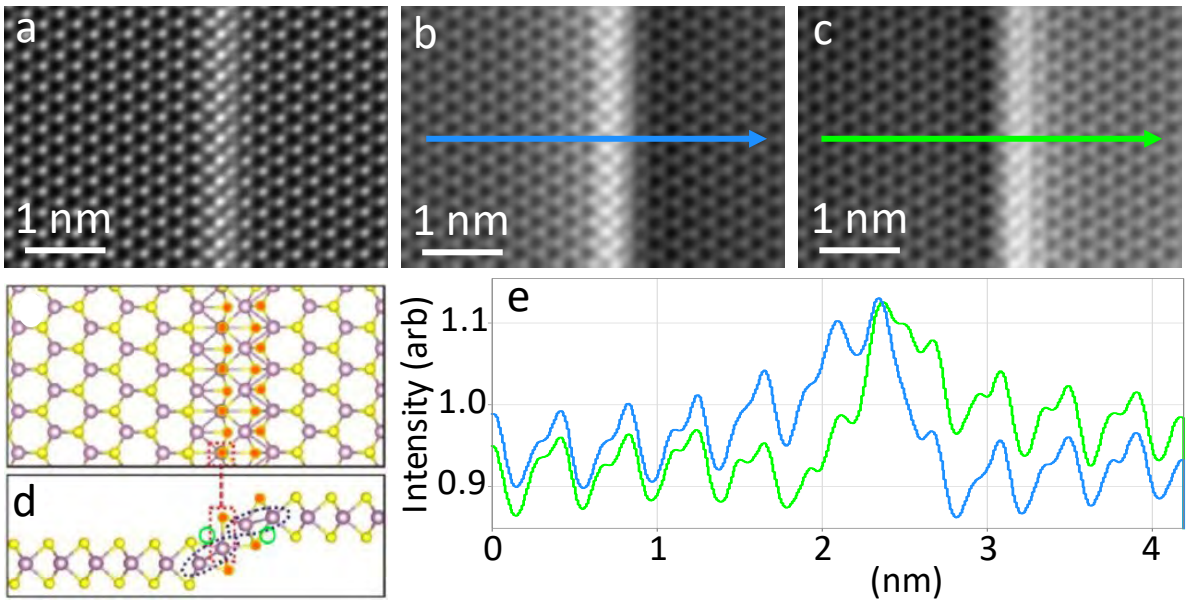

Fig 1. A line defect in MoS_2 imaged with (a) MAADF, (b, c) gaussian filtered entrance and exit side SE. The line defect has out-of-plane "buckled" structure (reproduced from ref. [3]) as shown in (d). The SE signal is sensitive to the local topography and inverts, left side bright vs right side bright, for the entrance and exit side detectors. The line profile shows the scale of this topography contrast compared to the atomic modulation of the SE signal. E_0=60 kV, 40 pA beam current, 35 mrad convergence half-angle, 323×478 pixels, net 1 ms/pixel.

References:
[1] Y. Zhu et al., Nature Materials **8** (2009) 808-812.
[2] M.T. Hotz et al., Microscopy and Microanalysis, 29 (Suppl 1), 2023, 2064–2065
[3] Q. Chen et al., ACS Nano **12** (2018), 7721-7730

Artificial Intelligence Compatible Charged Beam Optical System

Hiroyuki Ito[1, a], Nishi Ryuji[1], Jun Yamasaki[1]
[1] Osaka university, Japan
[a] e-mail hiirto-youkui@ozzio.jp

Electron optical system has been practically perfected for the development of various applications fields. As an example, the objective deflection optics with autonomous driving technology, was the core of electron beam lithography (EBL). From these experiences, further approaches for the electron optical system, that lead to artificial intelligence (AI) compatible designs, will be presented.
Specifically, we have developed;
(1) Hysteresis free *N* symmetrical line current (*N*-SYLC) aberration corrector
(2) High speed voltage superimposed (*V*-SYLC) beam deflector
(3) Charging free double aperture lens (DAL) electron mirror.
Based on their expected outstanding controllability, the convergence property will be dramatically improved for the electron beam systems, such as SEM, TEM, and analyzers.
The conventional spherical aberration correction requires at least a symmetrical magnetic 6-poles system. As a result, the structural complexity and the magnetic hysteresis will sacrifice its operability. On the other hand, a magnetic pole less 3-SYLC, in which all three identical current lines are paralleled to total magnetic field B=0 on the central axis. Due to this circulation property of magnetic field, a 6-pole field is formed in the vicinity of the axis. Furthermore, if inverted current lines are added to the middle of the current wire gaps, a double strength magnetic field can be formed. The important feature of the *N*-SYLC corrector is, there is no concern about magnetic saturation or aftereffect, and stronger magnetic field can be generated in the proximity of the current lines. Theoretically, the 5th order *N*-SYLC system has been analytically solved, and furthermore, if the annular coil magnetic field is superimposed as shown in Fig.1, the action effect of the multipole magnetic field can be increased [(1)].
About the energy filter DAL, the electron reflection points are placed in a central higher potential surface between double apertures. As a result, the DAL energy filter is worked on high repeatability without surface charging, and it is a very important issue for an accurate and compact energy analyzer [(2)].
Finally, the integrated AI compatible system will be discussed for that will create new concepts and further applications. In this early stage, the key technology will be the application of *N*-SYLC including beam shaping and the noise suppression in time domain by selectable use of DAL and *V*-SYLC. For deeper AI technologies, it is expected the autonomous operation for the best physical result, including tuning of electron beam dynamical controls for material interaction processes.
The research was challenged by many people supports, authors would like to express sincere gratitude.

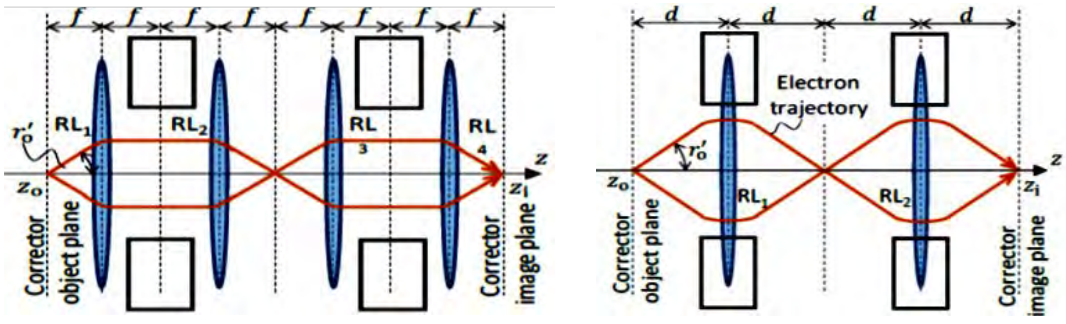

Figure 1. Conventional 6-pole and simplified in-lens 3-SYLC corrector

References:
[1] S. Hoque, R. Nishi, H. Ito, Spherical aberration correction with an in-lens *N*-fold symmetric line currents model, Ultramicroscopy, **87** (2018) 135-143.
[2] K, Honda, H. Ito, S. Katagiri, T. Doi, and M. Sasaki, A novel design of a retarding field electron energy analyzer with a cavity electrode providing extremely high energy resolution, JVSTB, **41**(4) (2023) 044006

Development of a Wire Corrector for Low Accelerating Voltage

Tomonori Nakano[1, a], Yu Yamazawa[2]
[1] Hitachi, Ltd. Research & Development Group, Japan
[2] Hitachi High-Tech Corporation, Japan
[a] tomonori.nakano.ut@hitachi.com

Electron microscopes with aberration correctors are widely used in innovative fields such as semiconductors, materials, and biological observations [1]. However, due to their cost and difficulty in control, they are not generally applied to conventional SEMs. To resolve these issues, a wire corrector has been developed [2-4]. The wire corrector is a type of multipole aberration corrector and consists of symmetrically arranged current lines on the optical axis, as shown in Figure 1. In this study, spherical aberration correction was demonstrated by a SEM equipped with a wire corrector and a bright-field STEM detector.

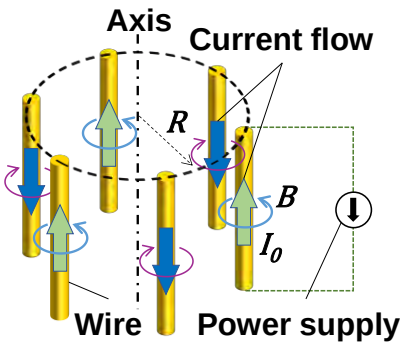

Figure 1. Schematic illustration of a wire lens.

Figure 2 shows BF-STEM images without and with spherical aberration correction. Since the interference is used to observe carbon multilayer at accelerating voltage of 30 kV, it is necessary to defocus from the minimum beam condition in the presence of spherical aberration [5]. On the other hand, the interference conditions and the beam minimum conditions coincide without spherical aberration, so the structure and carbon multilayer can be observed at the same time.

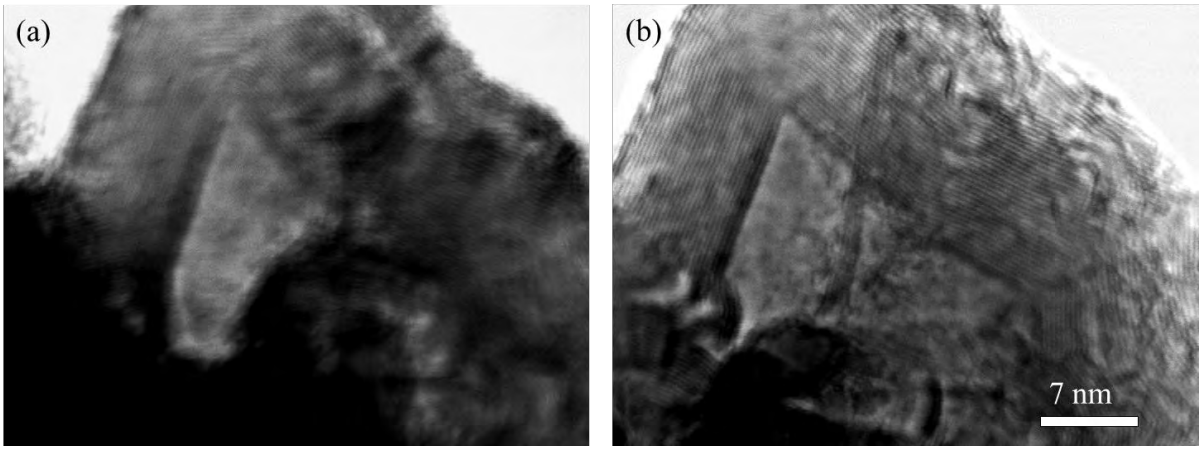

Figure 2. BF-STEM lattice images of graphite (a) without and (b) with aberration correction by a wire corrector at an accelerating voltage of 30 kV.

References:

[1] M. Haider et al., Advances in Imaging and Electron Physics Volume 153, p. 43 (2008)
[2] H. Ito et al., U.S. patent 7,872,240 (2011)
[3] S. Hoque et al., Ultramicroscopy 161, p. 74. (2016)
[4] T. Nakano et al., Journal of Vacuum Science & Technology B **37**, p. 012901. (2019)
[5] M. Konno et al, Ultramicroscopy 145, p. 28. (2014)

Wien Filter Application for Deflection Chromatic Aberration Correction in High-Resolution and Large-Field Low-Voltage Scanning Electron Microscopy

Kizawa, S. [1, a], Bizen, D. [1], Suzuki, K. [2], Mizutani, S. [2], Watanabe, R. [2], Kasai, Y. [2], Mizuhara, Y. [2]
[1] Hitachi, Ltd., Japan
[2] Hitachi High-Tech Corporation, Japan
[a] shun.kizawa.yf@hitachi.com

We present an approach in low-voltage scanning electron microscopy (LVSEM) to achieve high spatial resolution over a large field of view (FOV) by using a Wien filter to correct for deflection chromatic aberration. This aberration is a significant challenge in LVSEM, particularly when using the beam-image shift, a technique essential for achieving high spatial resolution over a large FOV at high speed. The presented approach utilizes the Wien filter to generate a compensatory deflection chromatic aberration that cancel out the one caused by the beam-image shift. Here, traditional methods of eliminating deflection chromatic aberration, such the use of a cold field emission gun [1], an aberration corrector [2], a monochromator [3], or a moving objective lens [4], are undoubtedly effective, but each has its own limitations, including emission current variations, complex power control requirements, loss of desired beam current, and high design and manufacturing costs. The Wien filter-based approach presented here is expected to be a practical and cost-effective option for correcting deflection chromatic aberration while avoiding these limitations.

As a demonstration, the maximum degradation in spatial resolution associated with a 28 µm × 28 µm of beam image shift was improved from 16% to 8% (Fig. 1). We also confirmed that the Wien filter responded 60% faster than the beam-image shift for the same amount of aberration, eliminating the need for additional settling time for correction. We also applied the technique presented to semiconductor pattern measurement and demonstrated its significant potential to enhance the critical dimension uniformity (CDU) within the FOV covered by the beam-image shift.

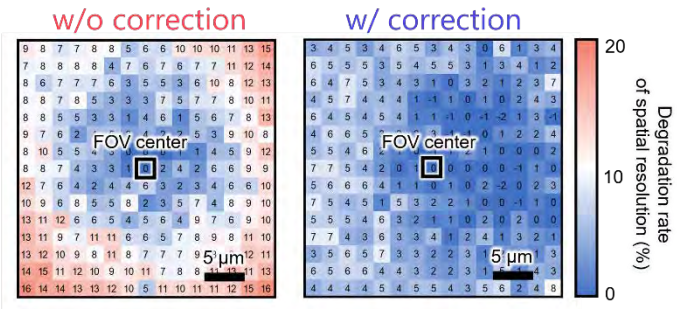

Figure 1. Distribution of the spatial resolution degradation in the FOV covered by the beam-image shift.

References:
[1] A. V. Crewe et al., Review of Scientific Instruments, **39**, 4, 576-583 (1968)
[2] J. Zach et al., Nuclear Instruments and Methods in Physics Research Section A: Accelerators, Spectrometers, Detectors and Associated Equipment **363**, 316 (1995).
[3] T. Ogawa et al., Microscopy and Microanalysis **28**, 412 (2022).
[4] H. Ohiwa, Journal of Vacuum Science and Technology **15**, 849 (1978).

Multireflection ASTRAL mass analyzer

Grinfeld, D.[1a], Stewart, H.[1], Hock, C.[1], Makarov, A.[1]
[1] Thermo Fisher Scientific, Bremen, Germany
[a] dmitry.grinfeld@thermofisher.com

Electrostatic mass analyzers may be divided into two groups according to the signal detection method. Fourier-Transform mass spectrometry (FT MS) instruments like the Orbitrap analyzer [1] and electrostatic bottles [2, 3] work with the induced-current detection, when the ions are set to make up to millions of oscillations. Their superior mass resolving power comes, however, at a price of a long analysis time. On the opposite, the time-of-flight (ToF) analyzers utilize very fast ion-impact detection upon a relatively short flight distance, but the mass resolution and sensitivity are moderate.

The development of gridless isochronous ion mirrors [4, 5] paved a road to the multi-reflection mass-spectrometry (MR MS) with a multiply folded ion path followed by an impact detection, which promises both high resolutions and repetition rates. The closed-path MR spectrometers with overlapping ion oscillations are successfully used, e.g. in nuclear physics [6]. They are not suitable, however, for analysis of complex mixtures, e.g. in biochemistry, because different ions undergo unknown numbers of reflections yielding an uninterpretable convoluted mass spectrum.

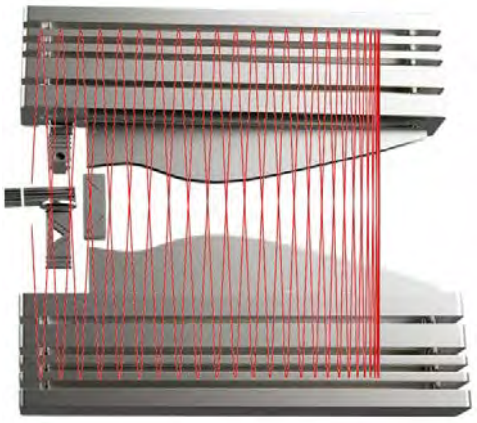

Figure 1. The ASTRAL mass analyzer

We tackled the problem of an open-path MR MS with a pair of elongated gridless mirrors, between which the ions make tens of oscillations while drifting in the direction of elongation. The ion motion is controlled in three dimensions with the major temporal and spatial ion-optical aberrations elaborately compensated. To this end, we implemented a drift control which incorporates reflections in the mirrors tilted towards each other at a small angle and refractions in specially shaped electrostatic prisms.

In our table-sized Asymmetric Track Lossless ASTRAL analyzer, shown in Figure 1, has the total length of flight circa 35m reached on 26 oscillations [7]. Two hundred mass spectra are obtained per second with the uniform mass resolving power over 100,000 in the full mass range. Optionally, the flight path may be repeated three times to enhance the resolution up to 250,000.

[1] A. Makarov. Anal. Chem. 72, 1156-62 (2000)
[2] D. Zajfman, et. al, Int. J. Mass Spectrom. 229, 55–60 (2003)
[3] T. Dickel, et al., Nucl. Instrum. Methods Phys. Res. A 777, 172–188 (2015)
[4] R. Kutscher, et. al., Int. J. Mass Spectrom. Ion Proc. 103, 117-128 (1991)
[5] H. Wollnik, et. al., Nucl. Instrum. Methods Phys. Res. A519, 373-379 (2004)
[6] M. Rosenbusch, et al, Nucl. Instrum. Methods Phys. Res. A1047, 167824 (2023)
[7] D. Grinfeld, et. al., Nucl. Instrum. Methods Phys. Res. A 1060, 169017 (2024)

Design of electron energy-loss spectroscope for SEM

Radlicka T.[1, a], Oral M. [1], Vlcek I. [1]

[1] Institute of Scientific Instruments of The CAS, v.v.i., Czech Republic
[a] radlicka@isibrno.cz

Energy Electron Loss Spectroscopy (EELS) with high spatial resolution is predominantly realized in conjunction with High-Resolution Scanning Transmission Electron Microscopy (HR-STEM). However, implementing EELS in a Scanning Electron Microscope (SEM) with the transmission mode could offer significant advantages: a) a stronger EELS signal at low primary beam energies, b) minimizing the generation of the Cherenkov radiation, which limits the determination of the forbidden bandgap in semiconductors, c) lower risk of sample damage.

We designed an EELS analyzer that can be fitted as an attachment to an existing SEM with an immersion objective lens (OL). The design of the EELS detector for Scanning Electron Microscopes (SEM) results from meticulous planning and consideration of several limiting and often contradictory requirements. We have carefully shielded the magnetic field of the immersion OL, which provides the ultimate resolution of the SEM. Another specificity is the absence of imaging elements, such as projection lenses or de-scan coils. The arrangement of components is also critical, as there is insufficient space beneath the sample holder. The sector magnet must bend the electron beam within the sample chamber, and the imaging tube must be routed through the specimen chamber's side wall or door.

The electron-optical design is inspired by O. Křivánek's paper [1]. It consists of a single sector magnet and four magnetic quadrupoles. A system of three magnetic hexapoles is employed to compensate for second-order aberrations. Additionally, the main third-order aberrations are corrected using two octupoles. Simulations show that the entire system will achieve an energy resolution of 0.2 eV which should allow accurate acquisition of energy-loss spectra. Our simulations also include an analysis of the required machining and alignment precisions and the necessary stability of electric current sources.

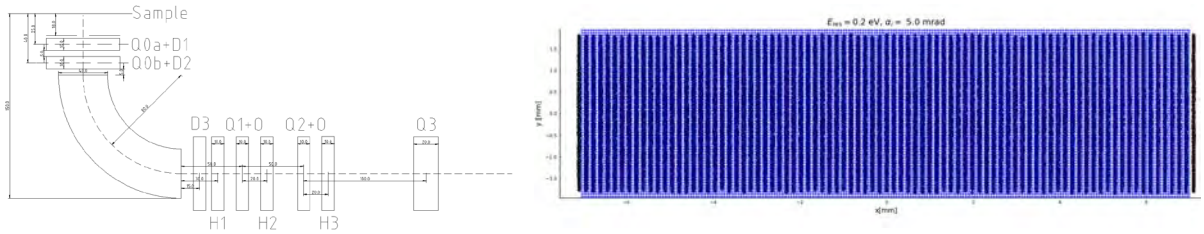

Figure 1. The electron optical schema of the EELS analyzer (left) and the separation of electron beams with an energy difference of 0.2 eV on the Timepix detector. The semiangle of the incoming beam into the analyzer was 5 mrad (right).

References:
[1] OL Krivanek, et al, Ultramicroscopy Vol 22, 103-116 (1987)
[2] The author acknowledges funding from the Technology Agency of the Czech Republic (project TN02000020).

Designing a quadrupole projection system for transmission SEM

Oral, M. [1a], Radlicka, T.[1]
[1] Institute of Scientific Instruments of the CAS, Czech Republic
[a] oral@isibrno.cz

Some commercially available scanning electron microscopes can be operated in the transmission mode with an annular detector of the transmitted electron beam below the sample. Such an SEM can be extended with a pixelated detector, allowing, at a low cost, 4D-STEM-like techniques, such as phase imaging or ptychography. A variable-magnification projection system imaging the diffraction plane onto the pixelated detector is ideally present to enable a variable camera length. However, the space constraints in specimen chambers of typical transmission SEMs make it difficult to accommodate such a projection system. Quadrupole multiplets can provide that in a more compact form than an optically comparable system consisting of round lenses at lower magnitudes of excitation voltages or currents.

The quadruplet is the simplest quadrupole multiplet allowing stigmatic (point-to-point) imaging to a given image plane at certain magnifications in both quadrupole's principal sections (potentially allowing an anamorphic image). An entirely analytical description of the paraxial imaging in a quadrupole multiplet is difficult due to the complexity of resulting expressions even if the thin-lens approximation is used [1]. We devised a semi-analytical computation approach to explore all available general non-trivial ray schemes of the quadrupole quadruplet. Based on solutions of the paraxial ray equation on FEM data from EOD [2] we characterize the focusing strengths and principal plane positions of each quadrupole as polynomial functions of the excitation. Then we can express the conditions for stigmatic imaging as a system of polynomial equations resulting from the appropriate drift and refraction steps between and at the principal planes of the quadrupoles. We solve the polynomial system using so-called homotropy continuation using a module for the Julia programming language [3]. The module also allows automated symbolic manipulations of the polynomial expressions prior to solving it. An example of one of the solutions is in Figure.

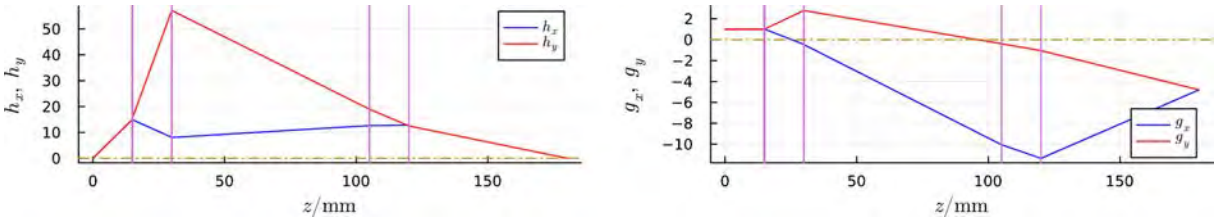

Figure: An example of imaging in a quadrupole quadruplet. Shown are the principal rays *h* and *g* in the two principal sections *xz* and *yz*. This system allows contiguous change of magnification from -0.75 to -4.8 (shown in figure for one of two nontrivial solutions). The vertical lines depict the principal planes of the 4 quadrupoles.

References:

[1] H. Rose: Geometrical Charged-Particle Optics, Springer-Verlag Berlin Heidelberg, 2012
[2] J. Zlámal, B. Lencová, Nucl. Instr. Meth. vol. 645, 278-282 (2011)
[3] P. Breiding, S. Timme, Intl. Congress on Math. Software, Springer, 458-465 (2018)
[4] The author acknowledges funding from the Technology Agency of the Czech Republic (project TN02000020).

Optimizing CPO instrument design in SIMION using simplex algorithm

Rathaiah Pureti[a], Tom Wirtz, Hung Hoang Quang
Advanced Instrumentation for Nano-Analytics (AINA), SIPT Unit, Luxembourg Institute of Science and Technology, 41 rue du Brill, L-4422 Belvaux, Luxembourg
[a] rathaiah.pureti@list.lu

The design and optimization of Charge Particle Optics (CPO) instruments are critical for advancing scientific and industrial applications such as microscopy, spectroscopy, and particle accelerators. These instruments require precise optimization of their design parameters to achieve high resolution, sensitivity, and accuracy. Optimizing potential distributions and the geometrical shapes of electrodes, apertures, and lenses involves traversing a complex, multidimensional parameter space.
SIMION, a valuable ion/electron optics simulation software, offers a robust platform for modeling and optimizing electrostatic and magnetic fields within CPO instruments [1]. Simplex optimization [2] is one of the optimization algorithms that are used with SIMION to improve the design and performance of CPO instruments. However, the typical workflow using the Simplex optimization algorithm in SIMION is limited by the number of parameters and a single objective that can be optimized, often converging to local minima rather than the global minimum due to its heuristic nature. Therefore, it is typically not sufficient to use SIMION with its Simplex optimization for optimizing complex multiple-parameters and multiple-objectives CPO systems.

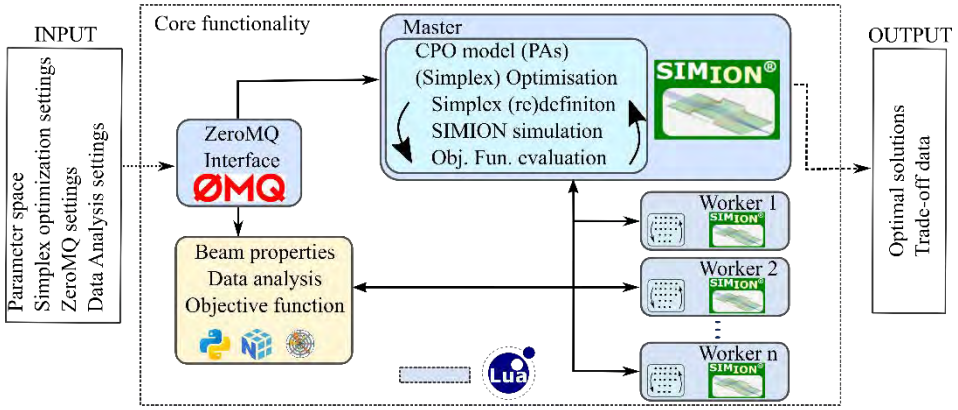

Figure 1.Framework diagram of the CPO Model optimization.

In this work, we adapt the Simplex optimization algorithm to optimize multiple parameters based on multiple objectives. This methodology is demonstrated by detailed case studies involving two and multi-electrode lens systems with up to six parameters, including both geometrical and potential parameters aspects of the electrodes. Objectives are focused on maximizing transmission and minimizing aberrations. To address the time-intensive nature of potential and field distribution calculations in complex or large systems, we also incorporate parallel processing to enhance computational efficiency (as shown in Figure 1). This approach provides a reliable methodology for complex CPO instrument design, balancing computational efficiency with high-precision results.

References

1. David A Dahl, International Journal of Mass Spectrometry, 200, 3-25 (2000).
2. Saša Singer and John Nelder, Nelder-Mead algorithm, Scholarpedia, 4(7):2928 (2009).

Acknowledgements

This work was supported by the Luxembourg National Research Fund (FNR) via the project, SIMS:ZERO (Grant No. BRIDGES2021/MS/15826187/SIMS:ZERO).

Image simulation in projection-type electron microscopy for understanding experimental images under practical conditions

Takeshi Morimoto[1, a], Momoyo Enyama[1], Yuta Kawamoto[2] and Akira Ikegami[2]
[1] Hitachi, Ltd., Japan
[2] Hitachi High-Tech Corporation, Japan
[a] takeshi.morimoto.sv@hitachi.com

When using projection-type electron microscopes such as TEM, LEEM, PEEM and MEM, images at various optical conditions are obtained. Though paraxial rays and aberration coefficients corresponding the optical conditions are calculated, image itself is not simulated in many cases. Therefore, it is difficult even for skilled electron optical designers to guess an image in a practical experimental condition, e.g., a condition where an aperture is inserted in an inappropriate position or the electron beam is off the center of the lens. From this point of view, an image simulation is still useful. However, an image simulation usually performed is based on raytracing and it is too time-consuming to calculate many optical conditions compared to paraxial rays and aberration calculations.

To address the problem, we performed image simulations based on paraxial rays and aberration coefficients. In the simulation, the position and velocity of the electrons on the sample are given, and the arrival position at the detector is calculated based on paraxial rays and aberration coefficients. Then, by calculating the arrival position for many electrons, an image is generated. As an example, we assume an optical system with two diffraction planes and also assume inserting angle limitation aperture at each planes. Schematic of the trajectory is shown in Fig. 1(a) and the simulated images are shown in Fig. 1(b). As shown in the figure, although the spatial resolution is improved by angle limitation in both the 1st and 2nd diffraction planes, only in the case of the 2nd diffraction plane, signal intensity at edge of the image decreases by aperture displacement. This is because the spread of h-trajectory is smaller and the tilt of g-trajectory is larger on the 2nd diffraction plane than on the 1st diffraction plane, resulting in a smaller tolerance on the aperture position. Although such an explanation is available from paraxial rays in Fig. 1(a), the image simulation allows a more intuitive and quantitative understanding. In our presentation, other results, e.g. images during lens wobbling under misalignment condition will be also reported.

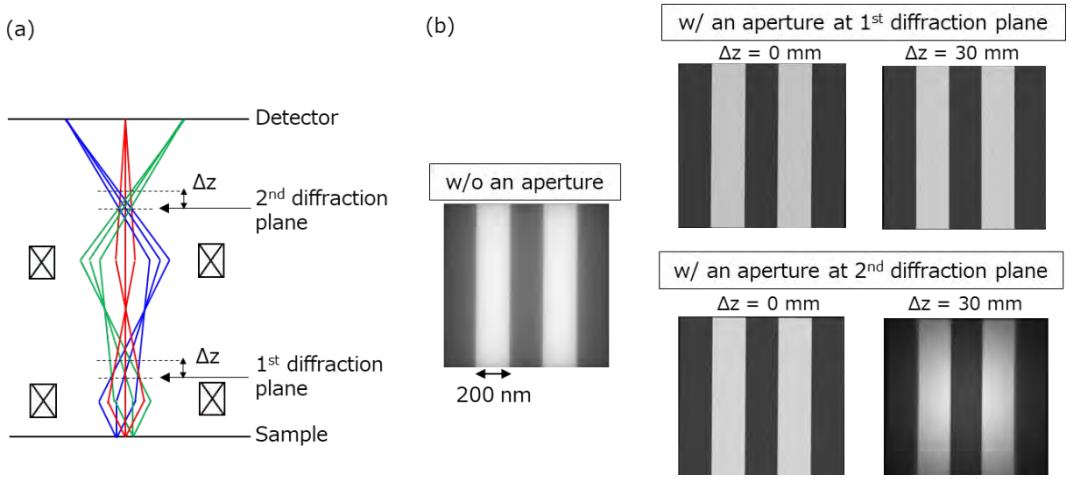

Fig. 1 (a) Schematic of paraxial rays of projection type electron microscope and positions of diffraction planes. (b) Simulated images where an angle limitation aperture is placed at different positions.

Evaluation Method of Image Sharpness in SEM Images with Edge Effect

Yoichi Ose[1, a], Shuangqi Dong [1]
[1] Hitachi High-Tech Corporation, Japan
[a] yoichi.ose.zp@hitachi-hightech.com

Managing SEM resolution is important for both SEM manufacturers and users, and it is necessary to evaluate the image sharpness with high accuracy. For this purpose, the Derivative (DR) method was proposed in 2007 [1]. This method treats the image as the convolution of the true object and the Gaussian point spread function and evaluates the image sharpness by fitting error functions to gradient directional edge profiles of particles in SEM images. However, the image sharpness tends to be underestimated in SEM images observed under high acceleration voltage due to edge effect [2].

To expand the range of applicable acceleration voltage, we propose the modified fitting function with edge effect (Figure 1).

Figure 2 shows a primitive result of the image sharpness of an artificial SEM image with and w/o considering edge effect.

We confirmed that underestimation of the image sharpness can be avoided by considering edge effect. At the conference, we will report the results of application to real SEM images.

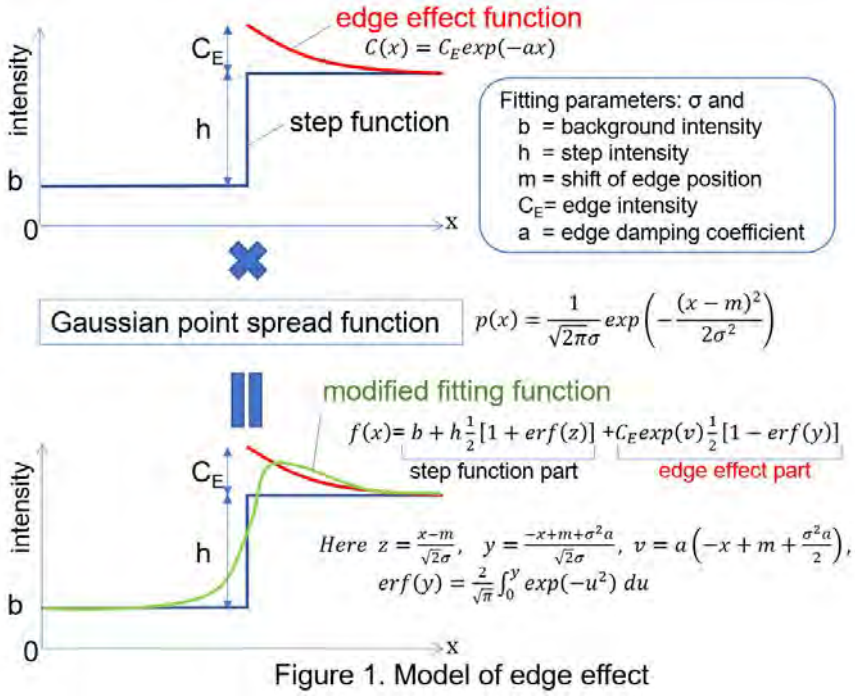

Figure 1. Model of edge effect

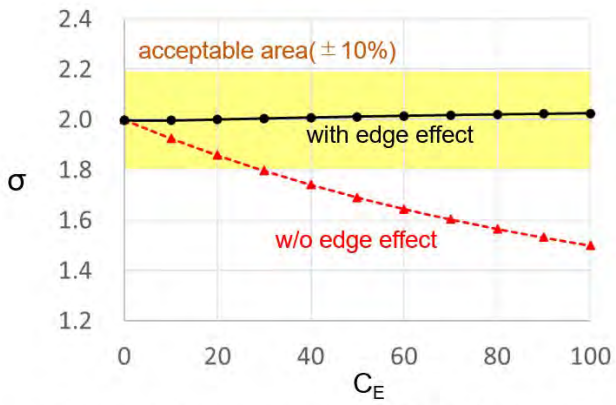

Figure 2. Improvement of σ estimation (a=0.2, σ=2, noise=0)

References:

[1] Bernd Rieger, The quest for higher resolution in optical and electron microscopy, Annual Meeting of the Dutch Society for Microscopy, 2007.
[2] P. Cizmar et al., Simulated SEM Images for Resolution Measurement, Scanning 30, 2008

I kindly acknowledge the helpful discussions with ISO/TC 202/SC4 members.

Evaluation of Virtual Source Size of NEA Photocathode by Knife-edge Method.

Daichi A. Takane[1, a], Hideo Morishita[1], Takashi Ohshima[2], Makoto Kuwahara[3], Toshihide Agemura[2], Yoichi Ose[2], Tsutomu Saito[2]
[1] Research & Development Group, Hitachi, Ltd, Japan
[2] Hitachi High-Tech Corporation, Japan
[3] Institute of Materials and Systems for Sustainability, Nagoya University, Japan
[a] daichi.takane.oy@hitachi.com

A scanning electron microscope (SEM) is a useful tool in many fields, including semiconductor devices, materials sciences, and biology. A pulsed SEM is a combination of SEM and a short-pulsed electron source that enables measurements with high spatiotemporal resolution. A promising candidate for an electron source for the pulsed SEM is a negative electron affinity (NEA) photocathode, which is a monochromatic pulsed electron source [1]. In a pulsed SEM equipped with the NEA photocathodes, the virtual source size of the electron source is sometimes a limiting factor in the spatial resolution. Additionally, the virtual source size is potentially increased by a Coulomb interaction between electrons in an electron beam. Thus, the effect of a Coulomb interaction on the virtual source size needs to be quantitatively evaluated. The main goals of this study are to develop a method to quantitatively evaluate the virtual source size of electron beams emitted from the NEA photocathodes and clarify the effect of the Coulomb interaction on it.

In this study, we employed a knife-edge method to measure the virtual source size of a nanosecond pulsed electron beam emitted from the NEA photocathode. The experimental setup is schematically illustrated in Figure 1(a). We mount a prototype electron gun on an SEM. The NEA photocahode is irradiated by a pulsed excitation light, which is focused to ~1 μm. An electron beam emitted from the NEA photocathode is focused onto a knife-edge by electron optics at a magnification (M) of 0.5 to 1.0. Scan coils are used to scan the electron beam across the knife-edge, and the amount of transemitted electron beams is measured as current (I_{pd}) by using a photodiode located below the knife-edge (Figure 1(b)). By using this system, we successfully determined the virtual source size of the NEA photocahode to be D_V~1.6 μm when Coulomb interaction is ignorable. This result is mostly consistent with the value estimated from the spatial resolution of the SEM image [2]. In our poster, we will show details of exprimental conditions and discuss the effect of a Coulomb interaction between electrons on the virtual source size.

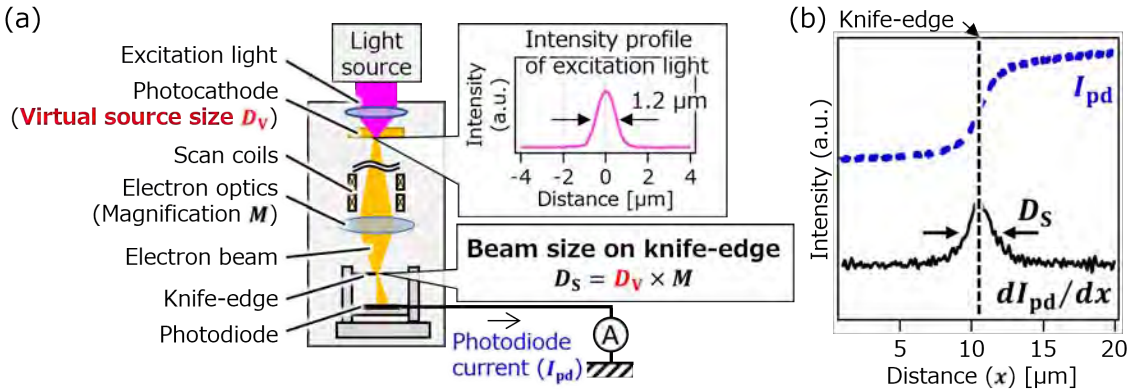

Figure 1. (a) Schematic of the experimental setup. (b) Example of experimental results.

References:
[1] M. Kuwahara *et al.*, Appl. Phys. Lett. **105**, 193101 (2014).
[2] H. Morishita *et al.*, J. Appl. Phys. **127**, 164902 (2020).

A gold needle tip array ultrafast electron source with high beam quality

Brückner, L. [1,a], Nauk, C. [1], Dienstbier, P. [1], Gerner, C. [1], Löhrl, B. [1], Paschen, T. [1], Heimerl, J. [1], Meier, S. [1], Hommelhoff, P. [1]
[1] Physics Dept., Friedrich-Alexander-Universität Erlangen-Nürnberg, Erlangen, Germany
[a] leon.brueckner@fau.de

Nanometer-sharp cold field emission tips are the electron sources with the highest beam quality. However, for a singular tip, the total emission current is limited. Combining the emission of multiple tips should allow for higher currents while preserving the properties of the individual emitters. Previous studies on tip arrays have already shown high currents and quantum efficiencies [1,2].

Here we introduce an ultrafast electron source composed of a lithographically fabricated array of nanometer-sharp gold tips (Figure 1) illuminated by 25 fs laser pulses [3]. By harnessing the emission of multiple needles, we achieve a high-current electron beam while preserving individual emitter properties. Our source delivers up to 2000 electrons per pulse at a laser repetition rate of 80 MHz, corresponding to 25 nA average current, with a narrow energy width of 0.5 ± 0.05 eV and a well-behaved Gaussian profile (Figure 2). The resulting electron beam exhibits high collimation and a small normalized emittance on the order of nm·rad, making it ideal for integration in compact electron-optical systems for applications requiring both high current and spatial resolution, such as free-electron light sources and chip-based particle accelerators. Additionally, we investigate the influence of strong-field effects on the electron emission from the arrays.

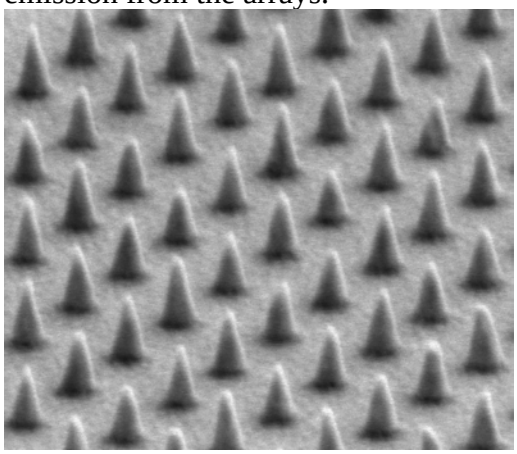

Figure 1: An array of lithographically fabricated gold needle tips. The tips are on average 110 nm tall and have a radius of curvature at the apex of 7.7 nm.

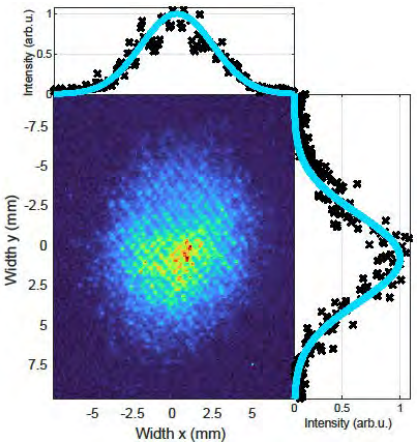

Figure 2: The transversal distribution of emitted electrons. The spot is Gaussian in both directions.

References:

[1] M. E. Swanwick, P.D. Keathley, A. Fallahi, P.R. Krogen, G. Laurent, J. Moses, F.X. Kärtner, L.F. Velásquez-García, Nano Letters 14, 5035–5043 (2014)
[2] S. Tsujino, P. Das Kanungo, M. Monshipouri, C. Lee & R.J. D. Miller, Nature Communications 7, 13976 (2016)
[3] L. Brückner, C. Nauk, P. Dienstbier, C. Gerner, B. Löhrl, T. Paschen, P. Hommelhoff, Nano Letters 24, 16, 5018–5023 (2024)

Relationship between the axial brightness of emitters and the spatial coherence length in TEM derived from the Wigner function

Shuhei Hatanaka[1, a] and Jun Yamasaki[1, 2]
[1] Research Center for Ultra-High Voltage Electron Microscopy, Osaka University, Japan
[2] Institute of Materials and Systems for Sustainability, Nagoya University, Japan
[a] hatanaka@uhvem.osaka-u.ac.jp

Field emission guns (FEG) and thermionic emission guns (TEG) are widely used as electron sources. Recently, photocathodes, which generates electron beams by laser irradiation, have been used in the field of ultrafast electron microscopy. Among these various electron emitters, the brightness and coherence of electron beams are the remarkable differences. In previous studies, we have quantitatively measured the spatial coherence of electron beams emitted from a Schottky FEG and a lanthanum hexaboride (LaB_6) TEG [1,2]. It is, however, difficult to compare the performance of the electron emitters using the coherence measurement results, because the spatial coherence depends on not only the electron emitter but also illumination lenses. In this study, we succeeded in deriving the formula to give the axial brightness of electron emitters based on the spatial coherence length.

In our previous studies, the spatial coherence of the electron beams has been measured by analyzing the intensity profiles of Airy patterns, which are the Fraunhofer diffraction pattern from a circular aperture [1,2]. In this method, not only the spatial coherence but also the amplitude and phase distributions of the electron beam can be determined. From these factors, the Wigner function $W(\boldsymbol{r}, \boldsymbol{q})$, which is a quasiprobability function in phase space spanned by the position and momentum bases, can be reconstructed [3]. Figure 1 shows an example of the reconstructed Wigner function of the electron beam emitted from a cold FEG. Using the value of the Wigner function at the origin and the electric current, the axial brightness B_0 is described as $B_0 = W(\mathbf{0}, \mathbf{0})k^2 I$ [4], where k and I are the wavenumber and electric current in phase space, respectively. Via the discussion of the Wigner function, we derived that the axial brightness is described as $B_0 = k^2 j l^2 / 2\pi$, where j and l are the current density and spatial coherence length in the specimen plane [3]. Using this method, the axial brightness of the cold and Schottky FEGs and the LaB_6 TEG were precisely evaluated [5].

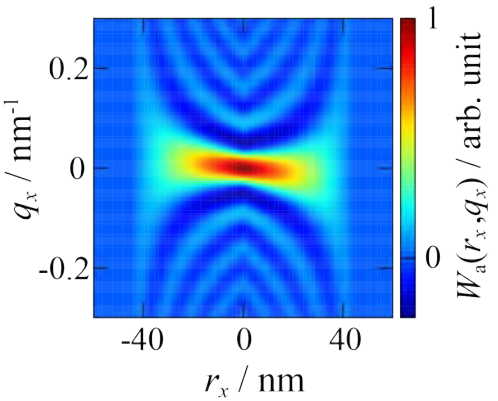

Figure 1. A reconstructed 2D Wigner function of the electron beam emitted from a cold FEG.

References:
[1] Jun Yamasaki et al., Microscopy **67**, 1-10 (2018).
[2] Shuhei Hatanaka and Jun Yamasaki, J. Opt. Soc. Am. A **38**, 1893-1900 (2021).
[3] Shuhei Hatanaka and Jun Yamasaki, Phys. Rev. A **110**, 013702 (2024).
[4] Alex Lubk and Falk Röder, Ultramicroscopy **151**, 136-149 (2015).
[5] Shuhei Hatanaka and Jun Yamasaki, Microscopy (2024) doi.org/10.1093/jmicro/dfae040
A part of this work was performed using the facility of the Institute of Materials and Systems for Sustainability (IMaSS), Nagoya University.

Electric field calculation on the field ion tip reconstructed from sequential FIM images

Jiayu Li[1,a], Tatsuo Iwata[1] and Shigekazu Nagai[1]
[1]Graduate School of Engineering, Mie University, Japan
[a] 424m250@m.mie-u.ac.jp

Field ion microscopy (FIM) can be used to observe atomic arrangements at the surface of needle metal samples with high spatial resolution (~0.2 nm). Therefore, FIM images contain information such as surface atomic arrangements, crystalline structures, and lattice defects. However, it is difficult to interpret the variation of intensity of each bright spot in FIM images, as it is influenced by several factors such as the electric field strength at the sample tip, the gas supply function, and the atomic species. The electric field strength at the surface can be calculated with atomic arrangement of the sample surface [1]. In this study, toward predictions of the atomic species from the intensity of bright spots in FIM images, we calculated the electric field strength assuming FIM sample with the ideal bcc structure. Also, we calculate a real sample model reconstructed with atomic positions extracted from FIM images.

As a first step, we constructed a sample model with an ideal bcc structure and curvature radius of 22 nm (Fig.1) and calculated its electric field strength. For the electric field calculations, each atom of the sample model was assumed to be a conductive rigid sphere, and the electron/ion optics design software SIMION 8.2, which utilizes the finite difference method, was employed. The critical distance is approximately 0.45 nm in the He-on-W system, and ionization of the imaging gas primarily occurs at this distance.[2] Fig. 2(a) and (b) show the electric field strength, obtained along a spherical surface at positions corresponding to 0.65 nm and 0.45 nm from the specimen surface, respectively, projected onto a plane assuming an opposing electrode. By comparing the FIM image (c) with the electric field strength distribution, it was confirmed that the crystal orientations in both are in good agreement. It was also revealed that the intensity of bright spots at the edge and terrace atoms shows a strong correlation with the electric field strength distribution.

In the next step, we will reconstruct a sample model using atomic arrangements extracted from FIM images and perform the electric field calculations for that model. To reconstruct the model, we examined an automatic extraction of the arrangement of the atoms based on the object classification and detection model (YOLO)[3]. The extracted atomic arrangement is then applied to a library that handles 3D models to generate the specimen model. The results of the electric field calculations will be discussed during the conference.

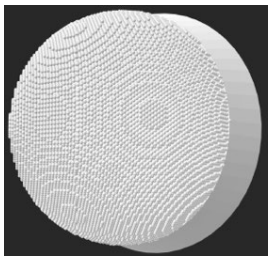

Figure 1. Model of the tip of the sample

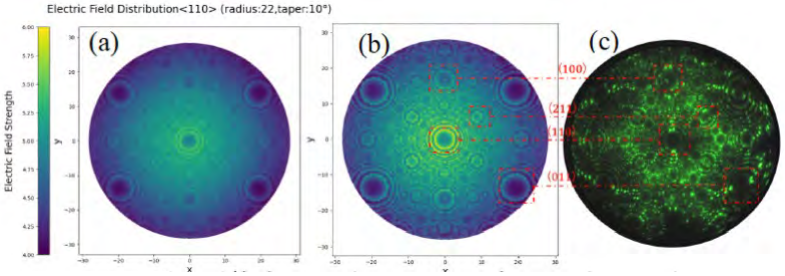

Figure 2. Comparison of W<110>FIM image and calculation results (a): Projection of electric field strength distribution (position equivalent to 0.65 nm from the tip) (b): Position equivalent to 0.45 nm from the tip (c): FIM image

References:

[1] F. Vurpillot, C. Oberdorfer. Ultramicroscopy.159, 202-216(2015).
[2] Baptiste Gault, et al. Atom Probe Microscopy. Springer. 9-13. (2012)
[3] J.Redmon, A. Farhadi, YOLOv3: An Incremental Improvement, UW, (2018)

Electron optics of the off-axial microlenses in microlens array

Hu J.T.*, Kang Y.F.
Key Laboratory for Physical Electronics and Devices of the Ministry of Education, School of Electronic Science and Engineering, Xi'an Jiaotong University, Xi'an, 710049, People's Republic of China
*e-mail: hujintao@stu.xjtu.edu.cn

The multi-electron-beam systems are developed to achieve the high throughput for electron microscope (EM). In these systems, the broad beam from the electron gun is usually split into sub-beams, i.e., axial sub-beam and off-axial sub-beams, and then focused by a microlens array (MLA) [1]. However, with the development of the multi-electron-beam systems, the array grows larger and the off-axial distances of the outer lenses in MLA increase, resulting larger aberrations for the off-axial sub-beams.

In this work we proposed a method, based on the differential algebraic (DA) theory, for calculating and analyzing the electron optical properties of the off-axial microlenses in MLA. The electron optics properties, e.g., aberration coefficients, are calculated numerically with respect to a practical, curved optic axis of the off-axial sub-beam passing through the off-axis microlens, as shown in Fig. 1. This optic axis is denoted as the reference trajectory that traced in DA method. In the process of solving this ray, the three-dimensional (3D) electric fields at an arbitrary point along the reference ray path are fitted into a series of appropriate polynomials [2]. The forms of these polynomials are determined by field components of the off-axial microlenses. These field components are numerically calculated by using the azimuthal Fourier analysis and Fourier-Bessel series [3]. In the case of off-axial microlenses, the field components are analyzed based on the central axis of each microlens. They are just the local harmonic components of the fields, which can be expressed by the global coordinate system:

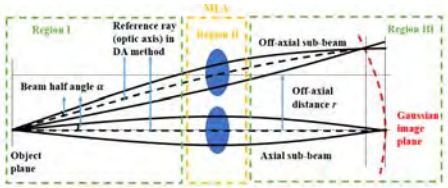

Figure 1. An off-axial sub-beam.

$$u(x,y)=\Phi_0-\frac{\Phi_0''}{4}\left[(x-x_0)^2+(y-y_0)^2\right]+\frac{\Phi_0^{(4)}}{64}\left[(x-x_0)^2+(y-y_0)^2\right]^2+\cdots,$$

where Φ_0 is the local rotationally symmetric field for an off-axial microlens in region II, and (x_0,y_0) is the center of the off-axial microlens. These field components are then transferred into DA arguments. Thus, the electron optics properties of the off-axial microlens are obtained by tracing only one reference ray in DA method. We note that the off-axial sub-beams do not possess a stigmatic focus in the Gaussian image plane of the axial sub-beam [4].

References:
[1] Mohammadi-Gheidari, A. et al., Nucl. Instr. And Meth. A, 645, 60-67 (2011).
[2] Yongfeng Kang, et al., Optik, 118, 158-162 (2007).
[3] Heerens, W. C., J. Appl. Phys., 53, 98 (1982).
[4] Berdnikov, A. S. et al., Nucl. Instr. And Meth. A, 363, 295-300 (1995).

Acknowledgements:
This work was supported by the National Natural Science Foundation of China (Grant No. 62071372) and the Natural Science Basic Research Program of Shaanxi (Program No. 2024JC-JCQN-69).

High accuracy measurement of multipole magnetic field

Abe, Tomohiko[2, a], Werber, Mathew[1], Sato, Yu[1], Kojima, Shinichi[1], Iwai, Toshimichi[2]
[1] Advantest America Inc., USA,
[2] Advantest Corporation, Japan
[a] tomohiko.abe@advantest.com

Multipole electron optical components such as Wien filter is composed of crossed magnetic and electric dipole fields. The fields are balanced for charged particles of a nominal energy, such that they experience no net force. Although simulations can be used to predict the strength and distribution of the magnetic field, a direct measurement of the actual magnetic field provides valuable insights. Recently we have measured the magnetic field of a Wien filter using a system consisting of a Hall probe with 3-axis measurement on one chip and high accuracy positioning. We obtained magnetic field vector data (Bx,By,Bz) at many x,y,z coordinates. Specifically the probe measures along the z axis with a 9x9 grid of x,y coordinates. Using a least square fitting routine we extracted the various field harmonics (dipole, quadrupole, hexapole, etc.)[1].
We found excellent dipole field uniformity with minimal higher order harmonics, suggesting no negative impact to beam quality. We also found that there was no saturation of the dipole field up to and above our expected operating current. Lastly, the dipole field profile matches the simulation very well. Overall, this indicates precise construction of the Wien filter, and we can expect it to operate as simulated.

References:
[1] Hawkes, Peter W., “6 Aberrations”, “Handbook of Charged Particle Optics (Second Edition)”, Jon Orloff (Editor), CRC Press (2009), 209-339.

Aberration analysis of magnetic sector energy filters by DA

Li M. S.*, Kang Y. F.

Key Laboratory of Physical Electronics and Devices, Ministry of Education, School of Electronic Science and Engineering, Xi'an Jiaotong University, Xi'an, 710049, People's Republic of China
*e-mail: lms960928@stu.xjtu.edu.cn

Imaging energy filters are widely used in transmission electron microscopes (TEMS) to improve resolution by further decreasing the energy spread of electron beams [1]. The most promising magnetic filters are called Ω filters, the optical axis of them are curved axis [2]. The traditional aberration analysis is based on sharp cut-off fringing field (SCOFF), which regards fringing field as analytical function to simplify the computation complexity. It is worth noting that fringing field effect should be analyzed more comprehensively in optimizing energy filters to obtain high resolution especially.

In this work, the differential algebraic (DA) method is introduced into the aberration calculation of an actual magnetic sector filter and Ω filter consisting of two magnetic sector units. The multipole fields are numerically calculated with respect to a practical, curved optic axis passing through the energy filters as shown in Fig. 2, as well as the electron optics properties. Based on curved optical axis and DA method, the multipole fields like dipole and quadrupole are taken into consideration, which can analyze fringing field effect deeply. The field components are transferred into DA arguments. Thus, the electron optics properties of the magnetic energy filters are obtained by tracing only one practical reference ray in DA method. To demonstrate the validation of method, the multipole field are equivalent to analysis function [3]. Furthermore, the optical properties of energy filer are computed in case of focusing in x-z plane.

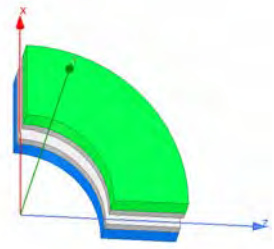

Figure 1. Schematic diagram of the sector energy analyzer

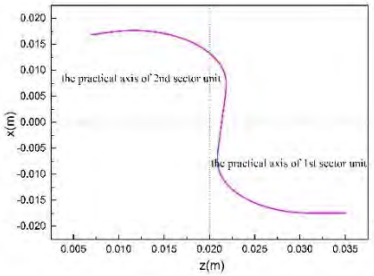

Figure 2. practical optical-axis of the sector energy analyzer

References:

[1] Rouse, John A., Eric Munro, and Katsushige Tsuno. Computer analysis of imaging energy filters. Charged Particle Optics III. Vol. 3155. SPIE, 1997.

[2] S. Lanio, H. Rose and D. Krahl. Test and improved design of a corrected imaging energy filter. Optik 73, P.56, 1986.

[3] Deininger, Christine, et al. Energy-filtering transmission electron microscopy. Vol. 71. Springer, 2013.

Development of an Improved Three-dimensional Boundary Charge Method Considering Space Charge Effects

Suzuki, Y., Murata, H. [a], Tanaka, T., Rokuta, E.
Faculty of Science and Technology, Meijo University, Tempaku-ku, Nagoya 468-8502, Japan
[a] hkmurata@meijo-u.ac.jp

Three-dimensional (3D) electron ray tracing that considers space charge effects is essential to evaluate the focal characteristics of medical X-ray tubes. We previously developed a 3D boundary charge method (BCM) applicable to various systems, including conducting, composite dielectric and magnetic systems [1, 2]. However, this BCM could not accommodate space charge effects. Herein, to achieve this, we propose an enhanced 3D BCM. The method is based on the idea that a virtual anode is introduced near the cathode, from the cathode to the virtual anode, the potential and electric field and current density in space are calculated using analytical methods, and from the virtual anode to the anode, the actual electron trajectory calculations are performed [3].

In the proposed method, the entire area from the cathode to anode is divided into two regions, as shown in Figure 1. In the first region (referred to as the analysis region), extending from the cathode ($z = 0$) to the virtual anode ($z = z_0$), the electron beam current, potential, and electric field in space are analytically calculated. Determination of whether the region is temperature-limited or space-charge-limited depends on the set cathode temperature. In the second region (referred to as the simulation region), from the virtual anode to the actual anode ($z = z_a$), the initial position and velocity of the electrons are derived from the analytically calculated potential and electric field at the virtual anode. Electron trajectory calculations are then conducted as though the electrons were emitted from the virtual anode. In this simulation, Coulomb forces due to space charges, placed at intervals of Δt along the electron trajectory according to the electron beam current, are considered. The calculations are iterated until convergence, resulting in the electron trajectory that is influenced by the space charge.

Figure 2 displays typical examples of electron ray tracing at cathode temperatures of (a) 2000 and (b) 3000 K for a parallel plate electrode model, with 0 and 130 kV applied to the cathode and anode, respectively. Notably, the electron trajectories exhibit slight divergence, attributed to variations in the cathode temperature.

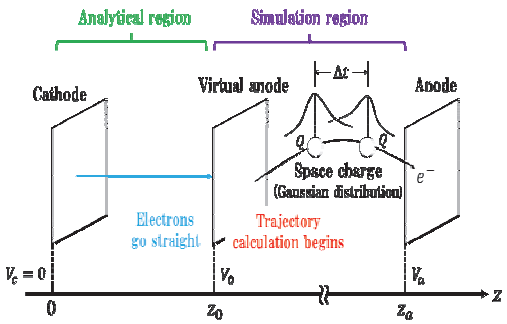

Figure 1. Schematic of the concept of reproducing space-charge effects.

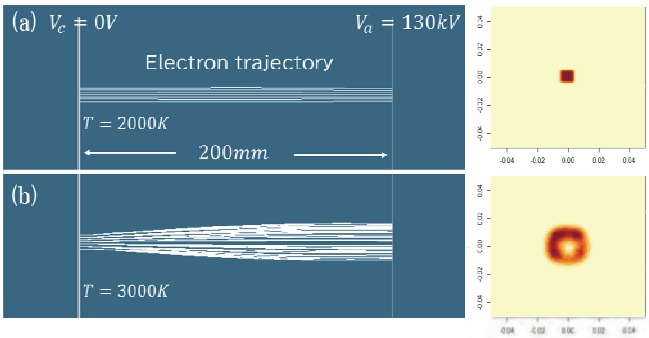

Figure 2. Examples of electron ray tracing (a) without and (b) with space charge effects.

References:

[1] H. Murata, T. Ohye, H. Shimoyama, Nucl. Instrum. Methods A **519** (2004) 184.
[2] H. Murata, M. Ishigami, H. Shimoyama, Nucl. Instrum. Methods A **806** (2016) 360.
[3] M. Fujita, M. Ohta, Shimadzu Hyoron (Shimadzu Review) **57** (2000) 67.

Probing Crystal Dislocations in Micrometer-Thick Semiconductor Specimens by High-Voltage Electron Microscopy

Kazuhisa Sato[1, a], Kotaro Hosono[2], and Shunya Takagi[1]
[1] Research Center for Ultra-High Voltage Electron Microscopy, Osaka University, Japan
[2] Division of Materials and Manufacturing Science, Osaka University, Japan
[a] sato@uhvem.osaka-u.ac.jp

Dislocations in semiconductor crystals degrade optical and electrical properties, so control of dislocation density is essential for practical applications. To detect and characterize lattice defects in a thick crystalline specimen which can be regarded as bulk, high-voltage transmission electron microscopy (HVEM) is a powerful technique. The penetration of MeV-electrons depends on imaging conditions as well as materials, and hence quantitative unified views regarding the maximum usable thickness have not been obtained so far. Recent interest in crystal defects in semiconductor devices has drawn renewed attention to visualizing microstructures in an extremely thick specimen by HVEM. The authors focused on high-voltage scanning transmission electron microscopy (STEM) as a tool for imaging dislocations in micrometer-thick crystals [1-3]. In this study, we employed the width of dislocation images as a criterion for the quantitative evaluation of usable thickness. We examined quantitative assessment of the maximum usable thickness of wedge-shaped GaN(0001) and 4H-SiC(0001) using HVEM operating at 1 MV.

Dislocations were observed using a JEOL JEM-1000EES operating at 1 MV. BF-TEM images were obtained using a 20 μm objective aperture with a semiangle of 2.8 mrad. BF-TEM images were recorded using a 2k × 2k charge-coupled device camera with an exposure time of 1–60 s. In the BF-STEM imaging, the beam convergence was set to a semiangle of 3.75 mrad using a 50-μm condenser aperture and the outer collection angle on the BF detector was set to 13 mrad. STEM images 1k × 1k in size were acquired with a dwell time of 256–1365 μs/pixel.

Threading dislocations in GaN were observed as lines with 15–20 nm width in a thickness range 1–4 μm by using BF-STEM [3]. We subjected specimens to a two-beam condition by exciting either the $1\bar{1}00$ or the $\bar{1}100$ reflection. Same dislocations were identified from both the front and back sides of the wedge-shaped specimen, regardless of the observation direction, when the thickness is less than 2.5 μm. To avoid ambiguity regarding the visibility of dislocations, we introduced a criterion for the evaluation of usable thickness: theoretical dislocation width ξ_{hkl} / π (ξ_{hkl} stands for the extinction distance of the *hkl* reflection excited for imaging) was employed as the criterion, and we judged data points below this line are "observable". Superior usable thicknesses in STEM than in TEM were found in the GaN specimen. The obtained results at 1 MV were as follows: 6.9 μm for STEM and 4.4 μm for TEM [3]. We show that the 1 MV-STEM is thus useful for imaging crystal defects in micrometer-thick semiconductor crystals. Recently, we have obtained similar results in 4H-SiC single crystals. The dependence of observable thickness on accelerating voltage and imaging mode (TEM, STEM, EFTEM) will also be presented at the conference.

References:
[1] K. Sato, Y. Yamashita, H. Yasuda, and H. Mori, *Jpn. J. Appl. Phys.* **56**, 100304 1-4 (2017).
[2] K. Sato, Y. Yamashita, H. Yasuda, and H. Mori, *Mat. Trans.* **60**, 675-677 (2019).
[3] K. Sato and H. Yasuda, *ACS Omega* **3**, 13524-13529 (2018).

The authors wish to thank Prof. J. Yamasaki of Osaka Univ. for invaluable comments. This study was partially supported by JSPS KAKENHI Grant Numbers 17H02746 and 21H05196.

Three-dimensional reconstruction of surface morphology of a polycrystalline dendrite particle using bright-field TEM images

Shinya Mizuno[1, a], Takeshi Nagase[2,3], Ryuji Nishi[3,4] and Jun Yamasaki[3,5]

[1] Department of Quantum Information Electronics, Osaka University.
[2] Department of Materials and Synchrotron Radiation Engineering, University of Hyogo.
[3] Research Center for Ultra-High Voltage Electron Microscopy, Osaka University.
[4] Department of Electrical and Electronics Engineering, Fukui University of Technology
[5] Institute of Materials and Systems for Sustainability, Nagoya University.
[a] mizuno@uhvem.osaka-u.ac.jp

Electron tomography is a method used for 3D morphological analysis of submicron-sized materials. A 3D volume is reconstructed from a set of electron microscopy images taken from various angles (tilt series). Accurate reconstructions require a linear relationship between the image signal and the sample thickness, typically seen in amorphous materials. However, crystalline materials show complicated contrast by Bragg diffraction (called diffraction contrast), complicating this relationship. In this study, we tried to develop a method for reconstructing the 3D surface of crystalline materials based on binarization processing for the tilt series of bright-field TEM images.

As a measurement target, we used a dendrite polycrystalline particle embedded in an amorphous Fe-Si-B alloy matrix. It is known that heating this alloy above 500°C results in growth of dendrite crystals therein. To understand the growth mechanism, 3D characterization of the growth front shape is important. As the dendrite particles are a few hundred nm in size, the matrix cannot be thinned below 500 nm, making observations by a common 200-kV TEM difficult. Thus, we used the ultra-high voltage electron microscope (Hitachi H-3000) operated at the acceleration voltage of 2000 kV, obtaining bright-field TEM images from 121 directions, -60° to +60° at 1° increments.

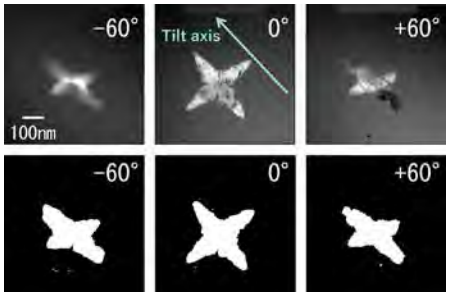

Figure 1: Tilt-series images of a dendrite polycrystalline particle (upper panels) and the binarized images (lower panels).

A few examples of the tilt-series images are shown in the upper panels of Fig. 1. To eliminate the complicated diffraction contrast, the images were binarized (lower panels), showing the crystalline particle clearly differentiated from surrounding amorphous regions. Figure 2 shows the 3D reconstruction results without and with the binarization. The overall surface morphology is clearly reconstructed with the binarization, apart from the elongation in some parts by the missing wedge effect (arrows). Compared to the noisy reconstruction in Fig. 2(d), the surface reconstructed with the binarization is sharp and smooth, allowing us to recognize the 3D curvature of the growth front (arrow in Fig. 2(h)).

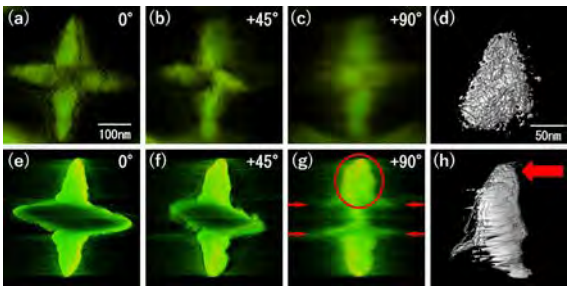

Figure 2: 3D reconstructions using the raw images (upper panels) and the binarized images (lower panels). (a)-(c) and (e)-(g) show volume rendering images viewed from the directions denoted at each upper right. (d) and (h) show surface rendering images of the encircled region in (g).

CPO-11 PARTICIPANTS

Baba, Susumu (Hitachi)

Berz, Martin (MSU)

Bizen, Daisuke (Hitachi)

Blackburn, Arthur M. (University of Victoria)

Breuer, John (Applied Materials)

Bruckner, Leon (Friedrich-Alexander University)

Chen, Xiya (Dongfang Jingyuan Electron)

Dellby, Niklas (Bruker)

Dohi, Hideto (Hitachi)

Enyama, Momoyo (Hitachi)

Fan, Fuyen (Ebara)

Fitzpatrick, Matthew R.C. (University of Victoria)

Fujita, Kunihiro (Samsung)

Fujita, Shin (Shimadzu)

Grinfeld, Dmitry (Thermo Fisher Scientific)

Haraguchi, Daisuke (Hamamatsu Photonics)

Hatanaka, Shuhei (Osaka University)

Hattori, Shinya (Hamamatsu Photonics)

Hirano, Yutaro (Hamamatsu Photonics)

Hu, Hangfeng (Xi'an Jiaotong University)

Hu, Jintao (Xi'an Jiaotong University)

Igari, Tomoya (Hitachi)

Ito, Hiroyuki (Osaka University)

Jiruse, Jaroslav (TESCAN)

Khan, Sameen A. (Dhofar University)

Khursheed, Anjam (Politecnico di Milano)

Kizawa, Shun (Hitachi)

Kojima, Shinichi (Advantest America)

Kuwahara, Makoto (Nagoya University)

Landers, David (CEA)

Li, Jiayu (Mie University)

Li, Shan M. (Xi'an Jiaotong University)

Luo, Yueting (Advantest America)

Maazouz, Mostafa (Thermo Fisher Scientific)

Makino, Kyoko (MSU)

Matsubara, Shinichi (Hitachi)

Matsuda, Kenji (University of Toyama)

Matsuoka, Genya (Lena-Systems)

Misima, Ryota (JEOL)

Mizuno, Shinya (Osaka University)

Morimoto, Takeshi (Hitachi)

Morimoto, Yuya (Riken)

Mullerova, Ilona (Institute of Scientific Instruments, CAS)

Murata, Hidekazu (Meijo University)

Nagai, Shigekazu (Mie University)

Nakano, Tomonori (Hitachi)

Ni, Dongdong (Dongfang Jingyuan Electron)

Nishi, Ryuji (Fukui University of Technology)

Nishiguchi, Masaru (Shimadzu)

Nishio, Tatsuya (Shimadzu)

Okamoto, Hiroshi (Akita Prefectural University)

Oral, Martin (Institute of Scientific Instruments, CAS)

Ose, Yoichi (Hitachi)

Pureti, Rathaiah (Luxembourg Institute of Science and Technology)

Radlicka, Tomas (Institute of Scientific Instruments, CAS)

Rouse, Catherine (Munro's Electron Beam Software)

Rouse, John A. (Munro's Electron Beam Software)

Saito, Eri (Hitachi)

Saito, Kosuke (Hamamatsu Photonics)

Sakakibara, Makoto (Hitachi)

Sato, Kazuhisa (Osaka University)

Sato, Yu (Advantest America)

Shibuya, Tatsunori (AIST)

Sun, Weiqiang (Dongfang Jingyuan Electron)

Suzuki, Yuto (Meijo University)

Takane, Daichi (Hitachi)

Taniguchi, Jun (Tokyo University of Science)

Valetov, Eremey V. (MSU)

Vasina, Radovan (Thermo Fisher Scientific)

Yamasaki, Jun (Osaka University)

Zhang, Lixin (IEE, Chinese Academy of Sciences)

Banquet

Wed., Oct. 16, 2024 18:00 to 20:00 at Kaikatei

Kaikatei is a Japanese restaurant where you can enjoy authentic kaiseki. The store and interior were designed by Kengo Kuma, a rare architect who is active all over the world. The architectural style, which boldly showcases superior architectural materials with meticulous precision, is directly connected to the concept of the cuisine.

Experience the atmosphere of the restaurant district and experience a new excitement about Fukui's food.

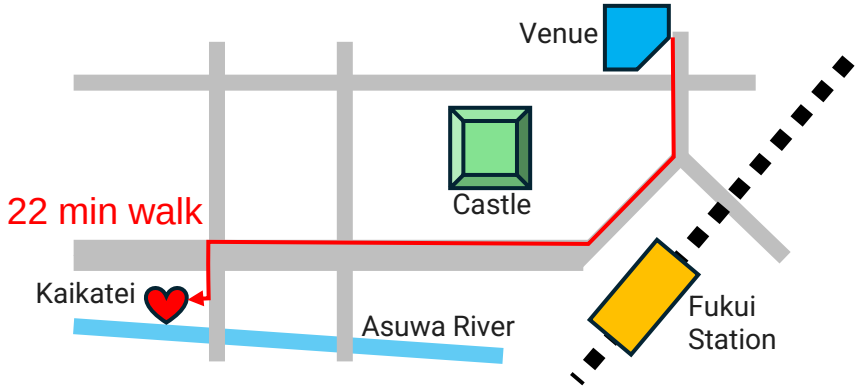

Excursion

Thu., Oct. 17, 2024 13:30 to 18:00 by bus

Boarding location: Fukui Station

East Exit (Ichijo Taniguchi) Platform

Meeting time: 13:20

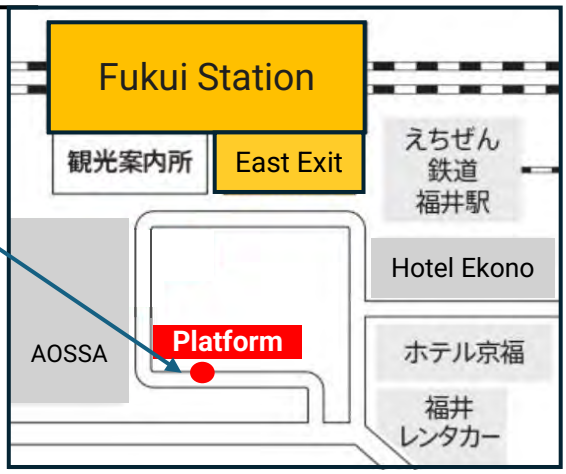

A course:

Fukui Prefectural Dinosaur Museum

Echizen Daibutsu

B course:

Daihonzan Eiheiji Temple

Ichijodani Asakura clan ruins restored townscape

Ichijodani Asakura Clan Ruins Museum